Article

Haematopoietic stem cell number is not solely defined by niche availability

https://doi.org/10.1038/s41586-025-09462-5

Received: 27 August 2023

Accepted: 28 July 2025

Published online: 27 August 2025

Open access

Check for updates

Shoichiro Takeishi[1,2]✉, Tony Marchand[1,2,15,16], Wade R. Koba[3], Daniel K. Borger[1,2], Chunliang Xu[1,2,17], Chandan Guha[4,5,6,7], Aviv Bergman[5,8,9,10], Paul S. Frenette[1,2,11,18,19], Kira Gritsman[1,2,7,12,13,14,18] & Ulrich Steidl[1,2,7,12,13,14,18]✉

Haematopoietic stem cells (HSCs) reside in specialized microenvironments, referred to as niches, and the classical model suggests that HSC numbers are predominantly determined by the niche size[1–5]. However, the vast excess of niche cells relative to HSCs challenges this perspective. To rigorously define the role of niche size in regulating HSC numbers, we developed a femur-transplantation system, enabling us to increase available HSC niches. Notably, the addition of niches did not alter the total HSC numbers in the body, suggesting the presence of a systemic mechanism that limits HSC numbers. Additionally, HSC numbers in transplanted wild-type femurs did not exceed physiological levels when HSCs were mobilized from defective endogenous niches to the periphery, indicating that HSC numbers are constrained at the local level as well. The notion of dual restrictions at systemic and local levels was further supported by other experimental approaches, including parabiosis and non-conditioned transfer of HSCs after bone transplantation. Moreover, we found that thrombopoietin has a pivotal role in determining the total number of HSCs in the body, even in the context of increased niche availability. Our study redefines key principles underlying HSC number regulation, providing insights into this critical biological process.

In the 1970s, Schofield proposed the niche model, suggesting that HSCs expand until they occupy their niches and HSC numbers are therefore predominantly determined by niche availability[5]. This idea is partially supported by the observation that transplanted HSCs do not engraft unless available niche 'space' is emptied by conditioning, such as irradiation, chemotherapy or other methods, which damages or mobilizes endogenous HSCs[5–10]. We and others have previously identified several HSC niche components, such as perivascular mesenchymal stem cells (MSCs), which are marked by nestin–GFP, *Cxcl12*^{GFP}, leptin receptor, or CD51 and CD140α expression[11–16]. It is also known that endothelial cells (ECs), characterized by the expression pattern of CD31, CD144, SCA-1 and CD62E, contribute to the HSC niche[11,17–19]. These cells produce niche factors, such as C-X-C motif chemokine ligand 12 (CXCL12) and stem cell factor (SCF, encoded by *Kitl*), which are essential for the retention and maintenance of HSCs in the bone marrow (BM). Genetic depletion of these cytokines or these HSC niches results in a reduction in HSC numbers in the BM[11–15,20,21]. One puzzling observation is that the number of defined niche cells is significantly greater than the number of HSCs[11,14–16]. However, these findings do not exclude the possibility that a small population of these niche cells creates unique saturable spaces, or that HSCs compete for space with their progenitors that also depend on niche factors. Notably, increasing evidence supports the notion that nutrition has a role in HSC maintenance both in culture and in vivo[22], suggesting the possibility that HSC numbers are determined by other mechanisms in addition to local control by niches. We therefore aimed to experimentally examine whether HSC numbers are indeed determined by niche availability in this study.

Bone transplantation adds new HSC niches

To rigorously define the role of niche size in regulating HSC numbers, we aimed to augment the overall availability of niches in vivo and to assess the impact of such a gain of niches on HSC numbers. To achieve this goal, we developed a bone transplantation method, transplanting femoral bones from one adult mouse to another[23,24]. In this model, when femurs (hereafter referred to as grafts) from wild-type (WT) mice

[1]Department of Cell Biology, Albert Einstein College of Medicine, Bronx, NY, USA. [2]Ruth L. and David S. Gottesman Institute for Stem Cell Research and Regenerative Medicine, Albert Einstein College of Medicine, Bronx, NY, USA. [3]Department of Radiology, Albert Einstein College of Medicine-Montefiore Medical Center, Bronx, NY, USA. [4]Department of Radiation Oncology, Albert Einstein College of Medicine-Montefiore Medical Center, Bronx, NY, USA. [5]Department of Pathology, Albert Einstein College of Medicine-Montefiore Medical Center, Bronx, NY, USA. [6]Department of Urology, Albert Einstein College of Medicine-Montefiore Medical Center, Bronx, NY, USA. [7]Montefiore Einstein Comprehensive Cancer Center, Albert Einstein College of Medicine-Montefiore Medical Center, Bronx, NY, USA. [8]Department of Systems and Computational Biology, Albert Einstein College of Medicine, Bronx, NY, USA. [9]Dominick P. Purpura Department of Neuroscience, Albert Einstein College of Medicine, Bronx, NY, USA. [10]Santa Fe Institute, Santa Fe, NM, USA. [11]Department of Medicine, Albert Einstein College of Medicine, Bronx, NY, USA. [12]Department of Oncology, Albert Einstein College of Medicine-Montefiore Medical Center, Bronx, NY, USA. [13]Blood Cancer Institute, Montefiore Einstein Comprehensive Cancer Center, Bronx, NY, USA. [14]Cancer Dormancy Institute, Montefiore Einstein Comprehensive Cancer Center, Bronx, NY, USA. [15]Present address: Service d'Hématologie Clinique, Centre Hospitalier Universitaire de Rennes, Rennes, France. [16]Present address: INSERM U1236, Université Rennes 1, Rennes, France. [17]Present address: Key Laboratory for Stem Cells and Tissue Engineering, Ministry of Education, Zhongshan School of Medicine, Sun Yat-sen University, Guangzhou, China. [18]These authors contributed equally: Paul S. Frenette, Kira Gritsman, Ulrich Steidl. [19]Deceased: Paul S. Frenette. ✉e-mail: shoichiro.takeishi@einsteinmed.edu; ulrich.steidl@einsteinmed.edu

are implanted subcutaneously into non-conditioned WT mice (called hosts), MSCs (marked by CD45$^-$TER-119$^-$CD31$^-$CD51$^+$CD140α$^+$)[16] persist in the grafts, while phenotypic HSCs (defined by Lin$^-$SCA-1$^+$KIT$^+$CD150$^+$CD48$^-$CD34$^-$)[25] and differentiated haematopoietic cells are no longer detected within 3 days after transplantation (Extended Data Fig. 1a–e and Supplementary Fig. 1a–f). For longer-term analyses, we next transplanted femurs from nestin–GFP transgenic mice[14] into nestin–GFP mice (one graft per host) (Extended Data Fig. 2a). We confirmed the overlap of nestin–GFP$^+$ cells and CD51$^+$CD140α$^+$ cells in the CD45$^-$TER-119$^-$CD31$^-$ fraction of the grafts, as previously reported for endogenous BM[16] (Extended Data Fig. 2b). Based on imaging, nestin–GFP$^+$ cells were observed in the grafts as well as in the host femurs at 1 and 5 months after transplantation, with robust vascularization shown by in vivo staining of the BM through CD31 and CD144 (Extended Data Fig. 2c). Flow cytometry analyses revealed progressive recovery of whole BM cells, MSCs and HSCs in the grafts (Extended Data Fig. 2d–f). However, while the host femurs and the grafts had comparable numbers of BM cells, MSCs and differentiated haematopoietic cells at 5 months after transplantation, HSC numbers in the grafts were still lower than those in the host femurs (Extended Data Fig. 2g).

We next examined the origin of MSCs, ECs and haematopoietic cells in the grafts. When femurs from nestin–GFP mice were transplanted into WT mice, most CD51$^+$CD140α$^+$ cells in the CD45$^-$TER-119$^-$CD31$^-$ fraction of the grafts were positive for nestin–GFP (Extended Data Fig. 3a,b). By contrast, nestin–GFP$^+$ cells were hardly detected in the CD51$^+$CD140α$^+$ fraction of WT grafts transplanted to nestin–GFP mice (Extended Data Fig. 3c,d), indicating that nestin–GFP$^+$ MSCs in the grafts originated from the grafts. Similar experiments were then performed using *Cdh5-creER;iTdTomato* (*Cdh5* encodes VE-cadherin) mice. Imaging and flow cytometry analyses confirmed TdTomato fluorescence in both arterial ECs (AECs; CD45$^-$TER-119$^-$CD31$^+$SCA-1^{high}CD62E^{low}) and sinusoidal ECs (SECs; CD45$^-$TER-119$^-$CD31$^+$SCA-1^{low}CD62E^{high})[19], regardless of whether *Cdh5-creER;iTdTomato* mice were used as hosts or grafts (Extended Data Fig. 3e–j), showing that these cells were derived from both the hosts and the grafts. Next, femurs from CD45.1 mice were transplanted into CD45.2 mice, and we observed that almost all BM cells, including HSCs, expressed CD45.2 (Extended Data Fig. 3k,l), indicating that haematopoietic cells in the grafts were replaced by the host cells. These results suggest that this femur transplantation system could be used to provide additional niches without adding HSCs.

Given that granulocyte colony-stimulating factor (G-CSF) mobilizes HSCs from the BM to the periphery[26], and HSCs in grafts are of host origin, we examined the effects of administration of G-CSF on the recovery of HSCs in grafts (Extended Data Fig. 4a). Imaging analyses at 3 months after transplantation revealed normal BM vascular architecture in the grafted femurs, as evidenced by comparable vascular density and arteriole lengths between the host and grafted femurs (Extended Data Fig. 4b–d). We did not observe any differences in nestin–GFP$^+$ density in imaging, which was further confirmed by flow cytometry analyses, demonstrating equivalent BM cellularity and frequency of nestin–GFP$^+$ cells in host versus grafted bones (Extended Data Fig. 4e–g). Similar observations were made when we performed the same experiments with WT hosts and grafts (Fig. 1a). BM cellularity, and the number of HSCs, differentiated haematopoietic cells, ECs and MSCs were again comparable between the host and grafted femurs at 3 months after transplantation with no significant differences in the frequencies of the stromal cell subsets (Fig. 1b–h). The levels of inflammatory cytokines (IL-1β, IL-6 and TNF) in BM extracellular fluid (BMEF) did not differ between these two types of bones at 2 or 3 months after transplantation, while the amount of IL-1β increased in the transplanted femurs at 1 month (Fig. 1i and Extended Data Fig. 4h), at which time HSCs were nearly absent in the grafts. Moreover, sorted MSCs from the hosts and the grafts at 3 months after transplantation expressed equivalent mRNA levels of canonical niche factors, such as *Cxcl12*, *Kitl*, *Vcam1*, *Angpt1* and *Spp1* (Fig. 1j and Supplementary Table 1), consistent with RNA-seq data in our recent study showing that MSCs from endogenous femurs and grafts express comparable levels of HSC niche-associated genes[23]. Protein levels of CXCL12 and SCF in BMEF also did not differ between the host femurs and the grafts (Extended Data Fig. 4i). Consistent with comparable niche function in the host and grafted femurs, HSCs from these two bones exhibited similar mean fluorescence intensity of KIT, CD150 and CD41, as well as cell cycle status and expression levels of cell cycle regulators, which were shown to be associated with HSC fates and functions[27–32] (Fig. 1k and Extended Data Fig. 5a,b). BM reconstitution assays using HSCs collected from either unperturbed femurs, host femurs or grafts at 3 months after bone transplantation showed comparable donor chimerism in the peripheral blood (Fig. 1l) and BM, which was maintained after secondary BM transplantation (BMT) (Extended Data Fig. 5c–g). Collectively, these results demonstrate that this femur transplantation system provides adult mice with additional functional niches, in which host-derived HSCs are able to engraft with minimal inflammatory stress and maintain multilineage reconstitution of the haematopoietic system.

HSC number restriction at the systemic level

Iron-distribution experiments estimate that one femur contains only 6–7% of the total BM in mice[33] and we observed that two femurs contain 16.9 ± 0.924% of HSCs in the total body (Extended Data Fig. 6a). Thus, to assess how an increase in the HSC niches affects total HSC numbers in the body, six WT femurs were transplanted per WT mouse, followed by G-CSF administration (Fig. 2a and Extended Data Fig. 6b). The mRNA expression of inflammatory cytokines in peripheral blood cells was not elevated at 3 months after transplantation (Fig. 2b). BM cellularity, EC and MSC numbers, and the levels of niche factors were comparable among the femurs from sham-operated mice, the host femurs and the grafts from bone transplantation hosts (Fig. 2c–e and Extended Data Fig. 6c–g). These data indicate that our six-femur transplantation technique enables us to add substantial HSC niches without inducing chronic systemic inflammation. HSC numbers in the grafts were independent of their transplanted sites and, notably, we found that the frequency and the absolute number of phenotypic HSCs per host femur and grafted femur were lower than those per femur from the sham-operated mice (Fig. 2f,g and Extended Data Fig. 6h). A BM reconstitution assay demonstrated lower donor chimerism when BM cells from the host femurs or the grafted femurs of bone transplantation hosts were transplanted (Fig. 2h). To determine whether such decreased repopulation activity was attributable to lower HSC numbers or a decreased competitiveness of HSCs, we performed competitive repopulation experiments with sorted HSCs. We found no difference in the repopulation activities among the three groups, consistent with equivalent mean fluorescence intensity of KIT and CD150 in transplanted HSCs (Fig. 2i and Extended Data Fig. 6i,j). These results suggest that the decreased BM repopulation activity in the host femurs and the grafted femurs from bone transplantation hosts resulted from a lower number of functional HSCs. Similarly, total HSC numbers in the entire body of bone transplantation hosts (excluding those in the grafts) were lower than those in the sham-operated mice (Fig. 2j). Importantly, the sum of HSC numbers in the bone transplantation hosts and the grafts was equivalent to that in the sham-operated group (Fig. 2k and Supplementary Table 2). These results indicate that the total HSC numbers in the body are not determined by niche availability alone, and suggest that their numbers are restricted at the systemic level (Extended Data Fig. 6k).

Given the increasingly clear role of multipotent progenitors (MPPs) in maintaining steady-state and stressed haematopoiesis[34–38], we also examined several subsets of MPPs[39] in this experimental system and found that MPP numbers per host femur and graft were lower than those per femur from the sham-operated mice (Extended Data Fig. 7a). MPPs in the entire body of bone transplantation hosts (excluding those

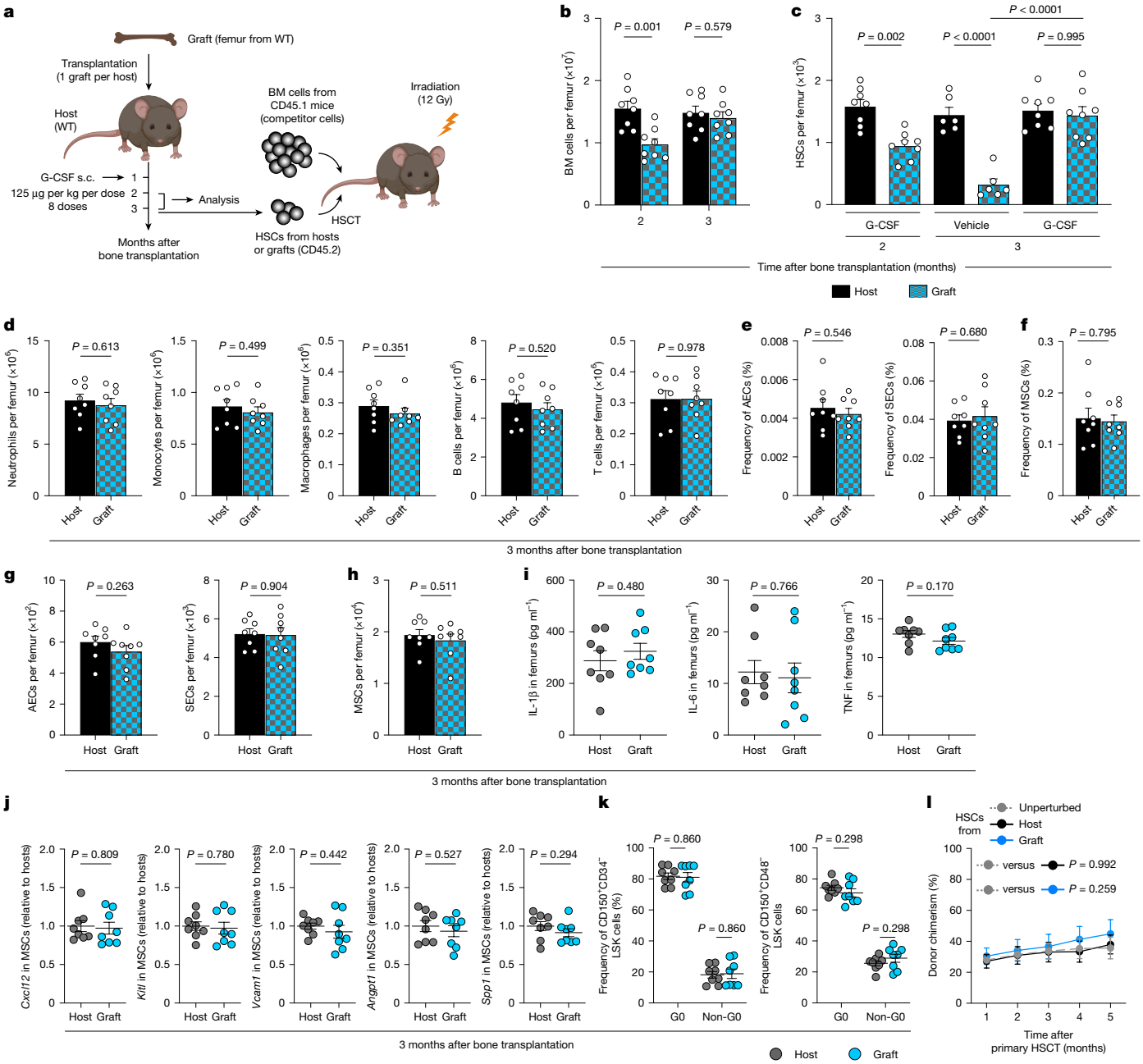

Fig. 1 | Normal functions of HSCs and their niches in the bone transplantation model. a, Experimental strategy and analyses for the transplantation of WT femurs into WT mice, G-CSF administration and HSC transplantation (HSCT). s.c., subcutaneous. The diagram was created using BioRender. Takeishi, S. (2025) https://BioRender.com/9d3nv16. **b**, BM cellularity per host femur and graft. $n = 8$ host femurs and 8 grafts from 8 G-CSF-administered host mice. **c**, HSC numbers per host femur and graft. $n = 6$ host femurs and 6 grafts from 6 vehicle-administered hosts, and 8 host femurs and 8 grafts from 8 G-CSF-administered hosts. **d**, The number of differentiated haematopoietic cells per host femur and graft. $n = 8$ host femurs and 8 grafts from 8 G-CSF-administered hosts. **e**,**f**, The frequency of ECs (**e**) and MSCs (**f**) in the host femurs and the grafts. $n = 8$ host femurs and 8 grafts from 8 G-CSF-administered hosts. **g**,**h**, The number of ECs (**g**) and MSCs (**h**) per host femur and graft. $n = 8$ host femurs and 8 grafts from 8 G-CSF-administered hosts. **i**, Inflammatory cytokine (IL-1β, IL-6 and TNF) levels in BMEF of the host femurs and grafts measured by enzyme-linked immunosorbent assay (ELISA). $n = 8$ host femurs and 8 grafts from 8 G-CSF-administered hosts. **j**, Quantification of mRNA levels of the indicated HSC niche factors in MSCs from the host femurs and grafts. $n = 8$ host femurs and 8 grafts from 8 G-CSF-administered hosts. **k**, The frequency of quiescent (G0) and proliferating (non-G0) cells in HSCs from the host femurs and grafts. $n = 8$ host femurs and 8 grafts from 8 G-CSF-administered hosts. **l**, White blood cell (WBC) chimerism (CD45.2) in recipient mice transplanted with HSCs (CD45.2) from unperturbed WT femurs, the G-CSF-administered host femurs or the grafts mixed with competitor BM cells (CD45.1). $n = 10$ mice per group. Data are mean ± s.e.m. Significance was assessed using a two-tailed unpaired Student's *t*-tests (**b** and **d**–**k**) or one-way analysis of variance (ANOVA; **c** and **l**).

in the grafts) were fewer than those in the sham-operated mice, and the sum of MPP numbers in the hosts and the grafts did not differ between these groups (Extended Data Fig. 7b,c). Collectively, MPP numbers in our six-femur transplantation model exhibit the same pattern as HSC numbers, suggesting that MPP numbers may also be subject to similar restrictions at the systemic level.

To further investigate whether HSC numbers are constrained systemically, we next sought to determine whether total HSC numbers

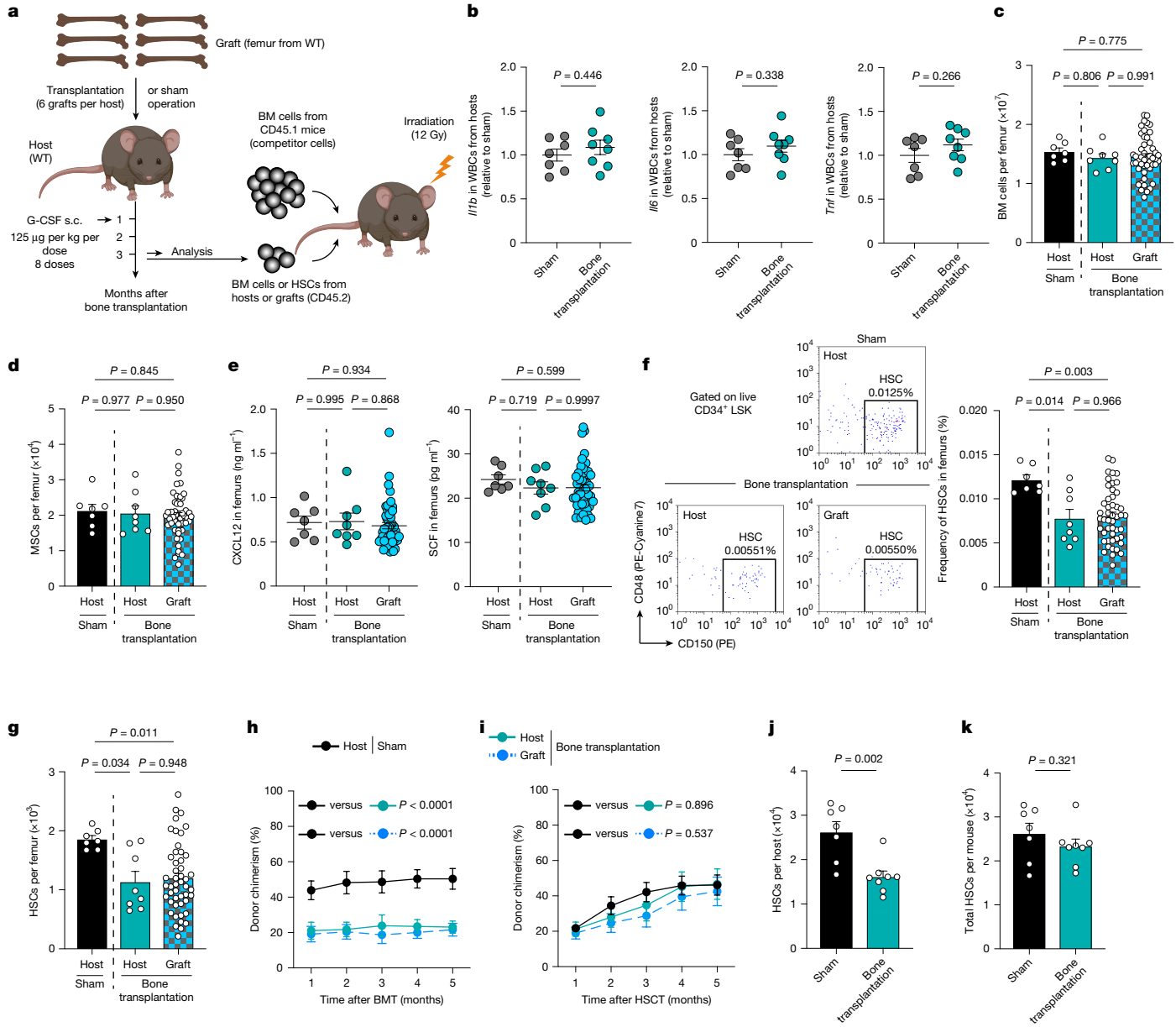

Fig. 2 | Unchanged total HSC numbers in the body after increased niche size. a, Schematic of the transplantation of six WT femurs into WT mice and analyses. The diagram was created using BioRender. Takeishi, S. (2025) https://BioRender.com/9d3nv16. **b**, Quantification of mRNA levels of the indicated inflammatory cytokines in WBCs from sham-operated mice and bone transplantation hosts. $n = 7$ and 8 mice, respectively. **c**,**d**, The number of BM cells (**c**) and MSCs (**d**) per host femur and graft. $n = 7$ femurs from 7 sham-operated mice, 8 host femurs and 48 grafts from 8 bone transplantation hosts. **e**, CXCL12 and SCF levels in BMEF of the host femurs and the grafts measured by ELISA. $n = 7$ femurs from 7 sham-operated mice, 8 host femurs and 48 grafts from 8 bone transplantation hosts. **f**, Representative flow cytometry plots of HSCs from the femurs of sham-operated mice, host femurs and grafts of bone transplantation hosts (left). Gates and percentages represent the frequency of the HSC population. Right, HSC frequency in the host femurs and the grafts. $n = 7$ femurs from 7 sham-operated mice, 8 host femurs and 48 grafts from 8 bone transplantation hosts. **g**, HSC numbers per host femur and graft. $n = 7$ femurs from 7 sham-operated mice, 8 host femurs and 48 grafts from 8 bone transplantation hosts. **h**,**i**, WBC chimerism (CD45.2) in recipient mice transplanted with BM cells (**h**) or HSCs (**i**) (CD45.2) from the indicated bones mixed with competitor BM cells (CD45.1). $n = 10$ mice per group. **j**,**k**, HSC numbers in the entire body of hosts (excluding grafts) (**j**), and the sum of HSCs in the hosts and the grafts (**k**). $n = 7$ and 8 mice, respectively. Data are mean ± s.e.m. Significance was assessed using two-tailed unpaired Student's *t*-tests (**b**, **j** and **k**) and one-way ANOVA (**c**–**i**).

in the body would be maintained in hosts that harbour defective endogenous niches. To this end, we used *Cdh2-creER;Cxcl12*$^{fl/fl}$ (*Cdh2* encodes N-cadherin) mice as hosts, given the known role of CXCL12 in the retention of HSCs in the BM[12]. Consistent with a study showing that *Cdh2*-expressing BM stromal cells contribute to the HSC niche[21], we observed that *Cdh2-creER;iTdTomato*$^{+}$ cells in the CD45^{-}TER-119^{-}CD31^{-} fraction largely overlapped with CD51^{+}CD140α^{+} cells and nestin–GFP^{+} cells (Extended Data Fig. 8a,b). HSC numbers were decreased in the BM and increased in the blood and spleens of *Cdh2-creER;Cxcl12*$^{fl/fl}$ mice (Extended Data Fig. 8c–e), indicative of extramedullary haematopoiesis. On the basis of this observation, six WT femurs were transplanted into *Cxcl12*$^{fl/fl}$ or *Cdh2-creER;Cxcl12*$^{fl/fl}$ mice before *Cxcl12* depletion by tamoxifen injection (Extended Data Fig. 8f). In the bone transplantation groups, HSC numbers per graft in *Cdh2-creER;Cxcl12*$^{fl/fl}$ (Cre^{+}) hosts were greater than those in *Cxcl12*$^{fl/fl}$ (Cre^{-}) hosts (Extended Data Fig. 8g), which could be attributable to more HSCs mobilized to the periphery in the former hosts. Notably, HSC numbers per graft in *Cdh2-creER;Cxcl12*$^{fl/fl}$ hosts are still lower than those in the femurs of sham-operated *Cxcl12*$^{fl/fl}$

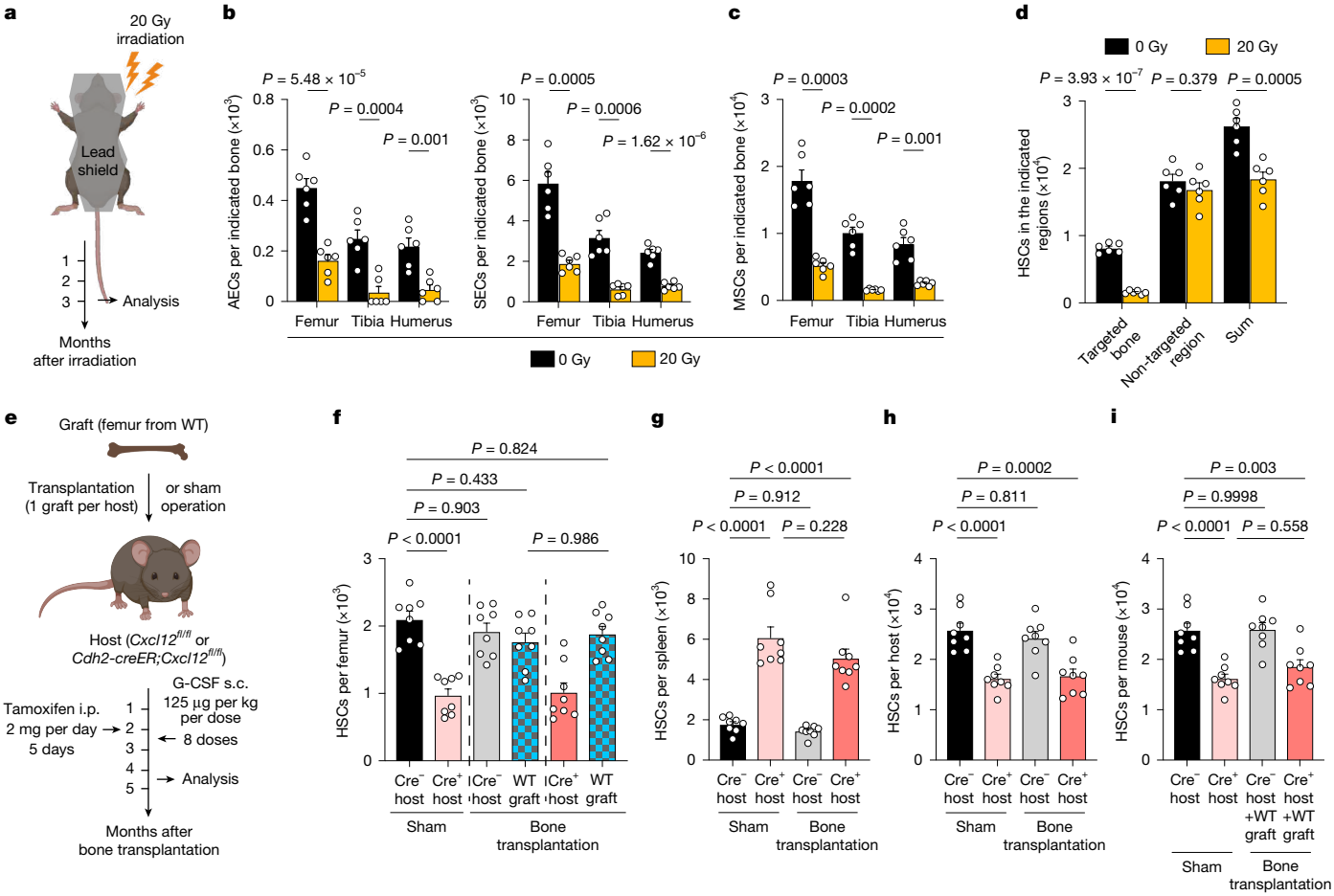

Fig. 3 | HSC numbers are limited locally. a, The experimental strategy and analyses for localized irradiation to limbs at a dose of 20 Gy. **b**,**c**, The number of ECs (**b**) and MSCs (**c**) in the targeted bones (limbs) after localized irradiation. $n = 6$ mice per group. **d**, HSC numbers in the targeted bones (four limbs), non-targeted regions (skull, spine, rib cage, pelvis, spleen and liver) and the sum of HSCs after localized irradiation. $n = 6$ mice per group. **e**, Schematic of the transplantation of a single WT femur into *Cdh2-creER;Cxcl12*$^{fl/fl}$ mice and analyses. i.p., intraperitoneal. **f**, HSC numbers per host femur and graft of the indicated genotypes. 8 femurs from 8 sham-operated mice, 8 host femurs and 8 grafts from 8 bone transplantation hosts in both *Cxcl12*$^{fl/fl}$ and *Cdh2-creER;Cxcl12*$^{fl/fl}$ groups. **g**–**i**, HSC numbers in the spleens (**g**) and in the entire body of hosts (excluding grafts) (**h**), and the sum of HSCs in the hosts and the grafts (**i**) of the indicated genotypes. $n = 8$ mice per group. Data are mean ± s.e.m. Significance was assessed using two-tailed unpaired Student's *t*-tests (**b**–**d**) and one-way ANOVA (**f**–**i**). The diagrams in **a** and **e** were created using BioRender. Takeishi, S. (2025) https://BioRender.com/9d3nv16.

mice, indicating that local HSC numbers in the former bones are below the physiological level. We also observed that bone transplantation mitigated extramedullary haematopoiesis in the spleens imposed by CXCL12 deficiency (Extended Data Fig. 8h). In the sham-operated groups, *Cdh2-creER;Cxcl12*$^{fl/fl}$ mice had fewer total HSCs than *Cxcl12*$^{fl/fl}$ mice (Extended Data Fig. 8i), which could be attributable, at least in part, to the insufficiency of extramedullary haematopoiesis in the spleens to compensate for the reduced HSC numbers in the BM. Notably, the sum of HSC numbers in *Cdh2-creER;Cxcl12*$^{fl/fl}$ hosts and WT grafts was equivalent to that in sham-operated *Cxcl12*$^{fl/fl}$ mice (Extended Data Fig. 8j). Collectively, these data suggest that total HSC numbers in the body remain unchanged when the size of the intact niche is increased, even in mice with impaired HSC retention in endogenous BM niches, further supporting the notion that HSC numbers are restricted at the systemic level (Supplementary Fig. 2).

Local limit on HSC numbers

To further characterize how HSC numbers are determined at the systemic level, we next examined whether damage to HSCs in one part of the body would be offset by an increase in HSCs in other regions. To this end, we subjected mice to targeted irradiation of their four limbs to permanently damage the niches and thereby eradicate HSCs in the limb bones, and then assessed HSC numbers in the non-targeted areas (Fig. 3a). At 3 months after irradiation with 20 Gy, we confirmed that EC and MSC numbers in the limb bones were reduced, while these cell numbers and expression levels of niche factors in the non-targeted bone were not affected by irradiation (Fig. 3b,c and Extended Data Fig. 9a–d). Although HSC numbers in the limbs were also decreased as expected, we did not observe any increase in HSCs in non-targeted areas (Fig. 3d and Extended Data Fig. 9e). There could be at least two possible explanations for this finding: (1) HSC numbers are restricted locally within each non-targeted bone (in addition to a limit on total HSC numbers in the body); and (2) HSC numbers are not upregulated when they are reduced in specific experimental settings. These two possibilities are not mutually exclusive.

To test the first hypothesis, we transplanted a single WT femur into *Cxcl12*$^{fl/fl}$ or *Cdh2-creER;Cxcl12*$^{fl/fl}$ mice (Fig. 3e), based on the assumption that the addition of only one femur would have a low impact on the total BM, and therefore HSC numbers in the grafts transplanted to *Cxcl12*$^{fl/fl}$ mice would reach physiological levels. We reasoned that, if there is no local restriction on HSC numbers, HSCs in the grafts would increase beyond the physiological level when HSCs are mobilized from endogenous BM to the periphery by CXCL12 depletion in the hosts.

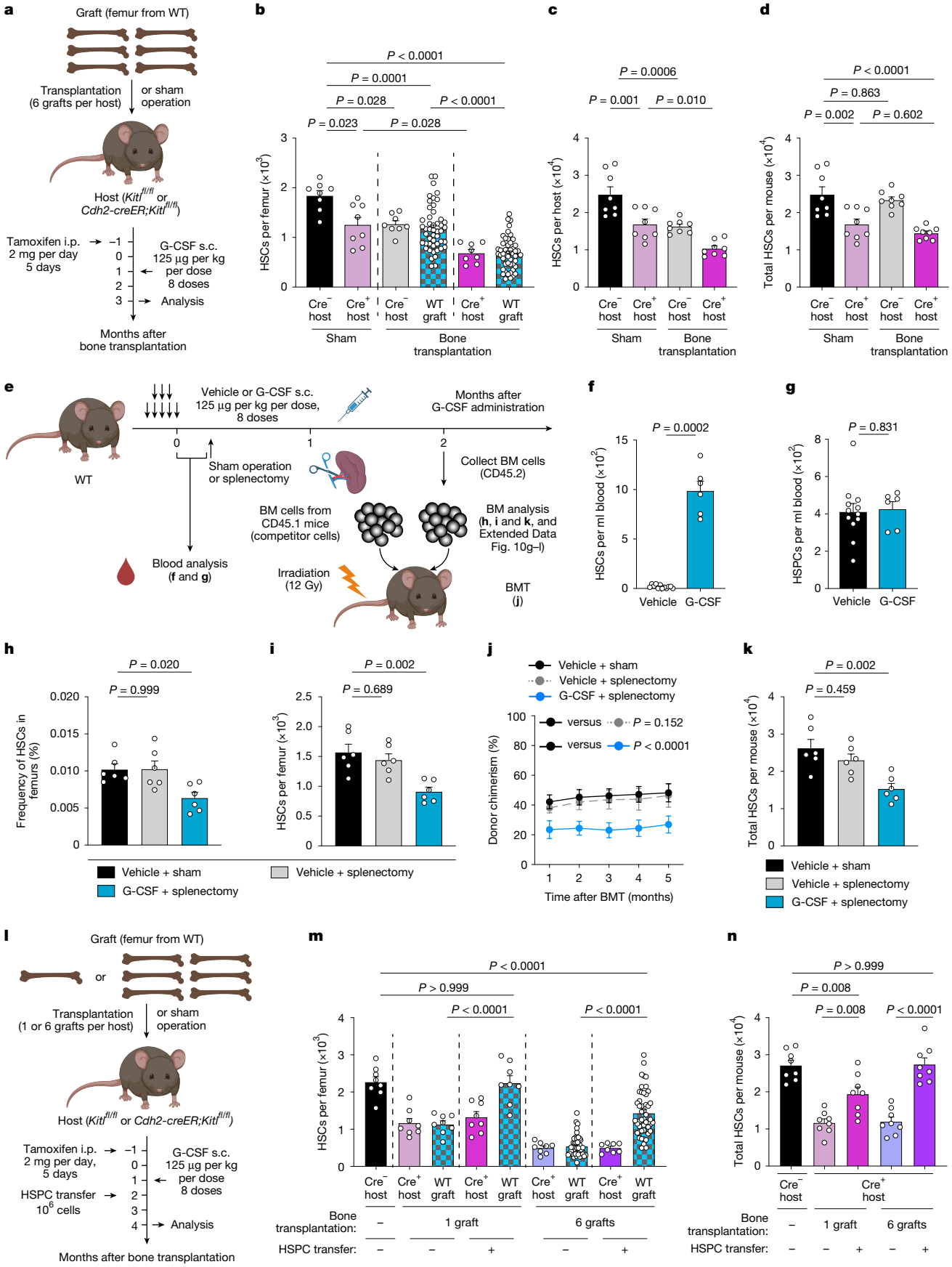

Fig. 4 | See next page for caption.

Fig. 4 | Homeostatic mechanism allowing for HSC replenishment. **a**, Schematic of six WT femur transplantation into SCF-deficient mice. **b**, HSC numbers per host femur and graft of the indicated genotypes. $n = 8$ femurs from 8 sham-operated mice, 8 host femurs and 48 grafts from 8 hosts in both *Kitl*$^{fl/fl}$ and *Cdh2-creER;Kitl*$^{fl/fl}$ groups. **c**,**d**, HSC numbers in the entire body of hosts (**c**) and the sum of HSCs in the hosts and the grafts (**d**) of the indicated genotypes. $n = 8$ mice per group. **e**, Schematic of G-CSF administration, followed by splenectomy and BMT. **f**, HSC numbers in the blood on the last day of G-CSF injection. $n = 12$ and 6 mice, respectively. **g**, HSPC numbers in the blood at 1 week after G-CSF administration. $n = 12$ and 6 mice, respectively. **h**,**i**, The HSC frequency (**h**) and numbers (**i**) in the femurs of the indicated cohorts at 2 months after G-CSF administration. $n = 6$ mice per group. **j**, WBC chimerism (CD45.2) in recipient mice transplanted with BM cells (CD45.2) from the indicated cohorts mixed with competitor BM cells (CD45.1). $n = 10$ mice per group. **k**, HSC numbers in the entire body of the indicated cohorts at 2 months after G-CSF administration. $n = 6$ mice per group. **l**, Schematic of WT femur transplantation and HSPC transfer into SCF-deficient mice. **m**, HSC numbers per host femur and graft of the indicated genotypes and conditions. $n = 8, 8, 8, 8, 8, 8, 48, 8$ and 48 bones, respectively. **n**, The sum of HSC numbers in the hosts and the grafts of the indicated genotypes and conditions. $n = 8$ mice per group. Data are mean ± s.e.m. Significance was assessed using two-tailed unpaired Student's *t*-tests (**f** and **g**) or one-way ANOVA (**b**–**d**, **h**–**k**, **m** and **n**). The diagrams in **a**, **e** and **l** were created using BioRender. Takeishi, S. (2025) https://BioRender.com/9d3nv16.

As expected, HSC numbers per host femur and grafted femur in *Cxcl12*$^{fl/fl}$ mice were comparable to those per femur of sham-operated *Cxcl12*$^{fl/fl}$ mice (corresponding to the physiological level) (Fig. 3f). However, CXCL12 deficiency in the host BM did not affect the HSC numbers per grafted WT femur. Consistent with these data, HSC numbers in the spleens of the hosts as well as in the host body (excluding the graft) were not altered by bone transplantation in the presence or absence of CXCL12 in the hosts (Fig. 3g,h). Notably, the sum of HSC numbers in the host body and the grafted WT femur of *Cdh2-creER;Cxcl12*$^{fl/fl}$ recipient mice was lower than that of sham-operated *Cxcl12*$^{fl/fl}$ mice (Fig. 3i), indicating that total HSC numbers in the former mice are below the systemic limit. Collectively, these data suggest that the failure to increase HSC numbers per graft in *Cdh2-creER;Cxcl12*$^{fl/fl}$ hosts is, at least in part, due to a local restriction on HSC numbers within the grafted femur (Supplementary Fig. 3).

To determine whether the findings of HSC number limitation at both systemic and local levels are reproducible using an alternative method, we next performed parabiosis experiments. Mice of the same or different genotypes (*Cxcl12*$^{fl/fl}$, *Cdh2-creER;Cxcl12*$^{fl/fl}$ and WT (CD45.1)) were surgically joined, and blood chimerism was analysed to confirm the exchange of circulating leukocytes between partners, followed by tamoxifen administration (Extended Data Fig. 9f,g). We found that the HSC numbers in the femurs from WT mice did not differ between the *Cxcl12*$^{fl/fl}$–WT pair and the *Cdh2-creER;Cxcl12*$^{fl/fl}$–WT pair (Extended Data Fig. 9h), suggesting a local restriction of HSC numbers in the BM. While splenic HSCs increased in both mice of the *Cdh2-creER;Cxcl12*$^{fl/fl}$–WT pair compared with the WT–WT pair, they were fewer than those in the pair of *Cdh2-creER;Cxcl12*$^{fl/fl}$ mice (Extended Data Fig. 9i), indicating that splenic HSC numbers in the *Cdh2-creER;Cxcl12*$^{fl/fl}$–WT pair were below their local limit in the spleen. Importantly, total HSC numbers per parabiont were equivalent between the *Cxcl12*$^{fl/fl}$–WT pair and the *Cdh2-creER;Cxcl12*$^{fl/fl}$–WT pair (Extended Data Fig. 9j). Taken together, these results suggest that HSC numbers in the *Cdh2-creER;Cxcl12*$^{fl/fl}$–WT pair are restricted at the systemic level, as well as locally in the BM, further supporting the notion that HSC numbers are limited at both systemic and local levels.

Homeostatic mechanism for HSC recovery

We also tested the second hypothesis, based on our observation in the targeted irradiation experiments, that HSC numbers are not upregulated when they are reduced in specific settings. To this end, we examined how HSC numbers are determined at the systemic level when local restriction on HSC numbers is lifted. We used *Cdh2-creER;Kitl*$^{fl/fl}$ mice as hosts, given that SCF is essential for the maintenance of HSCs in the BM[11,20]. Consistent with such a key role of SCF, we observed that tamoxifen-injected *Cdh2-creER;Kitl*$^{fl/fl}$ mice had fewer HSCs in the femurs, and equivalent numbers of haematopoietic stem and progenitor cells (HSPCs, defined by Lin$^-$SCA-1$^+$KIT$^+$ (LSK)) in the blood and HSCs in the spleens compared with *Kitl*$^{fl/fl}$ mice (Extended Data Fig. 10a–c). We then transplanted six WT femurs into tamoxifen-treated *Kitl*$^{fl/fl}$ or *Cdh2-creER;Kitl*$^{fl/fl}$ mice and found that HSC numbers per grafted femur in *Cdh2-creER;Kitl*$^{fl/fl}$ (Cre$^+$) hosts were further decreased compared with those in *Kitl*$^{fl/fl}$ (Cre$^-$) hosts, and HSC numbers in the hosts exhibited a similar trend (Fig. 4a–c). Notably, the sum of HSC numbers in the hosts and the grafts in *Cdh2-creER;Kitl*$^{fl/fl}$ hosts was equivalent to that in sham-operated *Cdh2-creER;Kitl*$^{fl/fl}$ hosts, but was lower than that in sham-operated *Kitl*$^{fl/fl}$ mice (Fig. 4d). Taken together, these data suggest that HSC numbers do not necessarily recover to physiological levels after they are reduced (Supplementary Fig. 4).

To exclude the possibility that the rescue of HSC loss at the systemic level requires SCF, we performed splenectomy after G-CSF administration to examine the impact of removing mobilized HSCs in the spleen on the number of residual HSCs in the BM (Fig. 4e). We observed more HSCs in the blood of G-CSF-treated mice compared with in vehicle-treated mice on the last day of G-CSF administration, and this was no longer evident in HSPC numbers at 1 week after G-CSF injection (Fig. 4f,g), indicating that HSC mobilization from the BM had concluded by this point. We also confirmed that G-CSF administration decreased HSC numbers in the BM at this timepoint, while increasing splenic HSCs (Extended Data Fig. 10d–f). Subsequently, we performed splenectomy or sham operation and analysed the BM at 2 months after G-CSF administration, based on a study showing that mobilized HSCs have returned to the BM 2 months after G-CSF treatment[26]. BM cellularity, EC and MSC numbers and the levels of niche factors, including SCF, were comparable among the vehicle + sham operation, the vehicle + splenectomy and the G-CSF + splenectomy groups (Extended Data Fig. 10g–l). Notably, we found that splenectomy after G-CSF treatment decreased the frequency and the absolute number of HSCs in the femurs, which was further confirmed by competitive repopulation assays of BM cells, while splenectomy alone did not affect these parameters (Fig. 4h–j). Similarly, the G-CSF + splenectomy group had a lower number of total HSCs in the body compared with the other two groups (Fig. 4k), demonstrating that HSC numbers do not necessarily recover when they are reduced, even when SCF is present.

To determine whether HSC replenishment is possible when their numbers are reduced, we next investigated the impact of non-conditioned transfer of excess HSCs into mice with fewer total HSCs in the body despite having intact niches. To this end, we expanded HSCs ex vivo[40] and transferred HSPCs (10^6 LSK cells per recipient mouse) into non-irradiated *Cdh2-creER;Kitl*$^{fl/fl}$ mice after the transplantation of one or six WT femurs (Fig. 4l). With single femur transplantation, although excess HSPC transfer restored HSC numbers in the grafts transplanted into SCF-deficient mice, their numbers per grafted femur did not increase beyond physiological levels (corresponding to the host femur of sham-operated *Kitl*$^{fl/fl}$ mice) (Fig. 4m). If there were no local restriction on HSC numbers, we would have expected higher HSC numbers per grafted femur than those at a physiological level, given that the number of transferred HSPCs vastly exceeded the number lost due to SCF deficiency in the endogenous niche. The sum of HSC numbers in *Cdh2-creER;Kitl*$^{fl/fl}$ hosts and WT grafts also increased after excess HSPC transfer, but remained below physiological levels (corresponding to sham-operated *Kitl*$^{fl/fl}$ mice) (Fig. 4n). Taken together, these results indicate that, in this setting, HSC numbers are limited

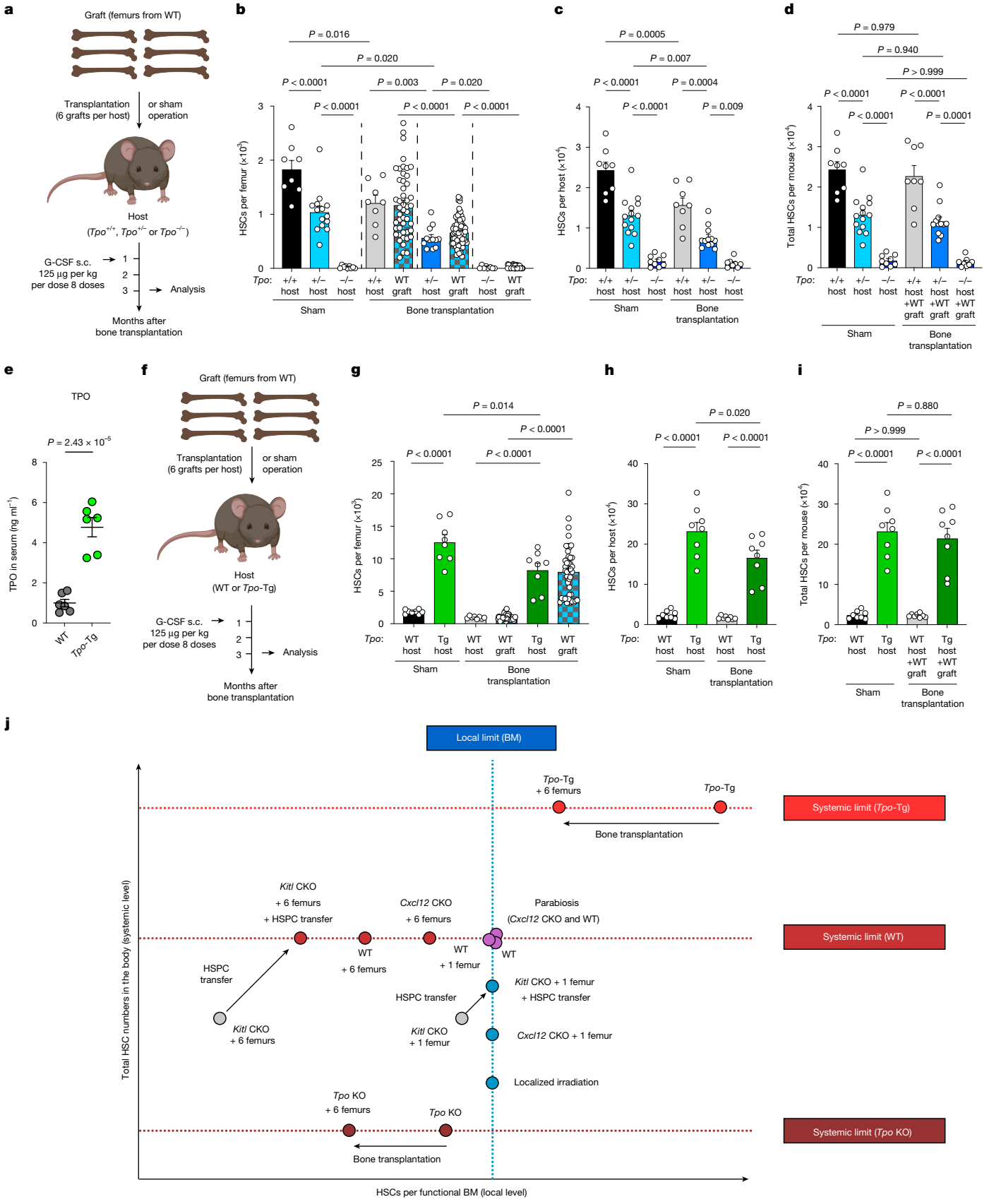

Fig. 5 | See next page for caption.

at the local level within the grafted femur. By contrast, when six WT femurs were transplanted into *Cdh2-creER;Kitl*$^{fl/fl}$ mice, excess HSPC transfer increased the number of HSCs per graft in these host mice, but their numbers were still below physiological levels. Although total HSC numbers in *Cdh2-creER;Kitl*$^{fl/fl}$ hosts and WT grafts also increased after excess HSPC transfer, they did not increase beyond physiological

Fig. 5 | TPO determines the total HSC numbers in the body in the context of increased niche availability. a, Experimental strategy for the transplantation of six WT femurs into *Tpo*-knockout mice. **b**, HSC numbers per host femur and graft of the indicated genotypes. $n = 8$ femurs from 8 sham-operated $Tpo^{+/+}$ mice, 14 femurs from 14 sham-operated $Tpo^{+/-}$ mice, 9 femurs from 9 sham-operated $Tpo^{-/-}$ mice, 8 host femurs and 48 grafts from 8 $Tpo^{+/+}$ hosts, 12 host femurs and 72 grafts from 12 $Tpo^{+/-}$ hosts, and 8 host femurs and 48 grafts from 8 $Tpo^{-/-}$ hosts. **c**,**d**, HSC numbers in the entire body of hosts (excluding grafts) (**c**) and the sum of HSCs in the hosts and the grafts (**d**) of the indicated genotypes. $n = 8, 14, 9, 8, 12$ and 8 mice, respectively. **e**, TPO levels in serum of WT and *Tpo*-Tg mice were measured using ELISA. $n = 6$ mice per group. **f**, Schematic of transplantation of six WT femurs into *Tpo*-Tg mice. **g**, HSC numbers per host femur and graft of the indicated genotypes. $n = 8$ femurs from 8 sham-operated mice, 8 host femurs and 48 grafts from 8 hosts in both WT and *Tpo*-Tg groups. **h**,**i**, HSC numbers in the entire body of hosts (excluding grafts) (**h**) and the sum of HSCs in the hosts and the grafts (**i**) of the indicated genotypes. $n = 8$ mice per group. **j**, Schematic of HSC numbers at local (x axis) and systemic (y axis) levels in each experimental approach. *Cxcl12* conditional knockout (CKO), *Cdh2-creER;Cxcl12*$^{fl/fl}$; *Kitl* CKO, *Cdh2-creER;Kitl*$^{fl/fl}$; *Tpo* KO, $Tpo^{+/-}$, $Tpo^{-/-}$. Data are mean ± s.e.m. Significance was assessed using two-tailed unpaired Student's t-tests (**e**) or one-way ANOVA (**b**–**d** and **g**–**i**). The diagrams in **a** and **f** were created using BioRender. Takeishi, S. (2025) https://BioRender.com/9d3nv16.

levels. These findings are consistent with the notion that HSC numbers are constrained at the systemic level. Collectively, these data suggest a homeostatic mechanism that allows for HSC replenishment when they are reduced, and is less permissive to their expansion after increased niche availability.

TPO levels set systemic HSC numbers

Lastly, we aimed to obtain mechanistic insights into the systemic limitation of HSC numbers. We hypothesized that signals from outside the BM, rather than factors from HSC niches, might be involved in this type of restriction. Among such long-range signals, we focused on thrombopoietin (TPO), based on its known role in the maintenance of BM HSCs[41,42]. To investigate whether TPO is able to constrain total HSC numbers in the body in the setting of increased niche availability, six WT femurs were transplanted into $Tpo^{+/+}$, $Tpo^{+/-}$ or $Tpo^{-/-}$ mice (Fig. 5a). In this experimental setup, if TPO primarily determines the level of HSC number restriction at the local level, we would anticipate that HSC numbers in host femurs and grafts from the bone-transplanted *Tpo*-knockout mice would be equivalent to those in femurs from their sham-operated controls of the same host genotypes, and thereby the former mice would have more HSCs in the entire body compared with the controls. We found that, in the sham-operated group, HSC numbers in femurs from $Tpo^{+/-}$ mice were lower than in $Tpo^{+/+}$ mice, with further reductions in $Tpo^{-/-}$ mice (Fig. 5b). Notably, HSC numbers per host femur and graft from the bone-transplanted $Tpo^{+/-}$ mice were lower than those per femur from the sham-operated $Tpo^{+/-}$ mice, and HSC numbers in the entire body of hosts (excluding those in the grafts) exhibited a similar trend (Fig. 5c). Importantly, the sum of HSC numbers in the hosts and the grafts did not differ between the bone-transplanted mice and their respective sham-operated controls of the same host genotypes (Fig. 5d), suggesting a role for TPO in determining the systemic limit of HSC numbers in the body, even in the setting of increased niche availability.

We also transplanted six WT femurs into *Tpo*-transgenic (Tg) mice, in which *Tpo* is overexpressed under the albumin promoter[43], or their littermate WT mice (Fig. 5e,f). In the sham-operated group, *Tpo*-Tg mice had more HSCs in the femurs than WT controls (Fig. 5g). HSC numbers per host femur from the bone-transplanted *Tpo*-Tg mice were lower than those from the sham-operated *Tpo*-Tg mice, and this trend was also evident in HSC numbers in the entire body of hosts (excluding those in the grafts) (Fig. 5h), making it unlikely that TPO primarily limits the local HSC numbers. The sum of HSC numbers in the hosts and the grafts did not differ between the sham-operated and the bone-transplanted *Tpo*-Tg mice, while they were significantly higher than physiological HSC numbers in WT hosts (Fig. 5i). Collectively, these data suggest that TPO levels have a key role in determining the level of restriction of total HSC numbers in the body, even in the context of increased niche availability (Fig. 5j and Supplementary Table 3).

Discussion

Here we used a femoral bone transplantation technique developed by our group that enables us to investigate the effect of increased niche size on HSC numbers. Data from transplanting six WT femurs into WT or CXCL12-deficient mice indicate that total HSC numbers in the body are maintained after the addition of normal niches, regardless of whether the endogenous niche is functional. This led us to conclude that HSC numbers are restricted at the systemic level. Further investigations, in which TPO levels were increased or decreased in the setting of six femur transplantation, suggest a pivotal role for TPO in determining the systemic limit of HSC numbers, even in the context of increased niche availability. In future studies, it will be interesting to evaluate whether elevated TPO levels affect HSC functions and/or create new niches. Moreover, several lines of evidence from other experiments, such as localized irradiation and single WT femur transplantation into CXCL12-deficient mice, suggest that HSC numbers are also limited at the local level within each specific intact niche. These restrictions at the systemic and local levels were further demonstrated by non-conditioned HSPC transfer after HSCs were decreased. These mechanisms of systemic and local restriction are not mutually exclusive, as further evidenced by our parabiosis experiments, which showed that HSC numbers in the *Cdh2-creER;Cxcl12*$^{fl/fl}$–WT pair are restricted systemically, as well as locally in the BM. On the basis of these findings, we propose that HSC numbers are restricted at both the systemic and local levels.

We also found that HSC numbers do not necessarily recover after they are reduced in specific conditions, including the bone transplantation system using SCF-deficient mice, unlike in stress haematopoiesis. In contrast to the disappearance of nearly all haematopoietic cells in the body after 5-fluorouracil challenge or BMT, BM cells persist in the body under the conditions tested in this study. The presence (in the case of localized irradiation, bone transplantation into SCF-deficient mice or G-CSF administration + splenectomy) or absence (after 5-fluorouracil challenge or BMT) of residual BM cells in the body might affect the distinct responses to HSC reduction in these settings. Given the recent notions that the majority of HSCs is dispensable for steady-state haematopoiesis[34–38] and that HSCs are involved in the pathogenesis of haematological malignancies as a source of (pre)leukaemic stem cells[44,45], it is intriguing to speculate that the haematopoietic system might be equipped with extrinsic safeguards that suppress HSC numbers to prevent leukemogenesis, even at a slight expense for normal haematopoiesis. It has been reported that HSC niche cell numbers are increased in myeloid malignancies[46,47]. In future studies, it may be interesting to determine whether the mechanisms of HSC number regulation are affected in these or other pathophysiological conditions.

Online content

Any methods, additional references, Nature Portfolio reporting summaries, source data, extended data, supplementary information, acknowledgements, peer review information; details of author contributions and competing interests; and statements of data and code availability are available at https://doi.org/10.1038/s41586-025-09462-5.

1. Calvi, L. M. & Link, D. C. The hematopoietic stem cell niche in homeostasis and disease. *Blood* **126**, 2443–2451 (2015).

2. Crane, G. M., Jeffery, E. & Morrison, S. J. Adult haematopoietic stem cell niches. *Nat. Rev. Immunol.* **17**, 573–590 (2017).
3. Pinho, S. & Frenette, P. S. Haematopoietic stem cell activity and interactions with the niche. *Nat. Rev. Mol. Cell Biol.* **20**, 303–320 (2019).
4. Scadden, D. T. Nice neighborhood: emerging concepts of the stem cell niche. *Cell* **157**, 41–50 (2014).
5. Schofield, R. The relationship between the spleen colony-forming cell and the haemopoietic stem cell. *Blood Cells* **4**, 7–25 (1978).
6. Bhattacharya, D., Rossi, D. J., Bryder, D. & Weissman, I. L. Purified hematopoietic stem cell engraftment of rare niches corrects severe lymphoid deficiencies without host conditioning. *J. Exp. Med.* **203**, 73–85 (2006).
7. Bhattacharya, D. et al. Niche recycling through division-independent egress of hematopoietic stem cells. *J. Exp. Med.* **206**, 2837–2850 (2009).
8. Chen, J. et al. Mobilization as a preparative regimen for hematopoietic stem cell transplantation. *Blood* **107**, 3764–3771 (2006).
9. Czechowicz, A., Kraft, D., Weissman, I. L. & Bhattacharya, D. Efficient transplantation via antibody-based clearance of hematopoietic stem cell niches. *Science* **318**, 1296–1299 (2007).
10. Tomita, Y., Sachs, D. H. & Sykes, M. Myelosuppressive conditioning is required to achieve engraftment of pluripotent stem cells contained in moderate doses of syngeneic bone marrow. *Blood* **83**, 939–948 (1994).
11. Ding, L., Saunders, T. L., Enikolopov, G. & Morrison, S. J. Endothelial and perivascular cells maintain haematopoietic stem cells. *Nature* **481**, 457–462 (2012).
12. Ding, L. & Morrison, S. J. Haematopoietic stem cells and early lymphoid progenitors occupy distinct bone marrow niches. *Nature* **495**, 231–235 (2013).
13. Kunisaki, Y. et al. Arteriolar niches maintain haematopoietic stem cell quiescence. *Nature* **502**, 637–643 (2013).
14. Mendez-Ferrer, S. et al. Mesenchymal and haematopoietic stem cells form a unique bone marrow niche. *Nature* **466**, 829–834 (2010).
15. Omatsu, Y. et al. The essential functions of adipo-osteogenic progenitors as the hematopoietic stem and progenitor cell niche. *Immunity* **33**, 387–399 (2010).
16. Pinho, S. et al. PDGFRα and CD51 mark human nestin+ sphere-forming mesenchymal stem cells capable of hematopoietic progenitor cell expansion. *J. Exp. Med.* **210**, 1351–1367 (2013).
17. Itkin, T. et al. Distinct bone marrow blood vessels differentially regulate haematopoiesis. *Nature* **532**, 323–328 (2016).
18. Kusumbe, A. P. et al. Age-dependent modulation of vascular niches for haematopoietic stem cells. *Nature* **532**, 380–384 (2016).
19. Xu, C. et al. Stem cell factor is selectively secreted by arterial endothelial cells in bone marrow. *Nat. Commun.* **9**, 2449 (2018).
20. Asada, N. et al. Differential cytokine contributions of perivascular haematopoietic stem cell niches. *Nat. Cell Biol.* **19**, 214–223 (2017).
21. Zhao, M. et al. N-cadherin-expressing bone and marrow stromal progenitor cells maintain reserve hematopoietic stem cells. *Cell Rep.* **26**, 652–669 (2019).
22. Schonberger, K. & Cabezas-Wallscheid, N. How nutrition regulates hematopoietic stem cell features. *Exp. Hematol.* **128**, 10–18 (2023).
23. Marchand, T. et al. Periosteal skeletal stem cells can migrate into the bone marrow and support hematopoiesis after injury. *eLife* **13**, RP101714 (2025).
24. Picoli, C. C. et al. Whole bone subcutaneous transplantation as a strategy to study precisely the bone marrow niche. *Stem Cell Rev. Rep.* **19**, 906–927 (2023).
25. Cabezas-Wallscheid, N. et al. Identification of regulatory networks in HSCs and their immediate progeny via integrated proteome, transcriptome, and DNA methylome analysis. *Cell Stem Cell* **15**, 507–522 (2014).
26. Bernitz, J. M., Daniel, M. G., Fstkchyan, Y. S. & Moore, K. Granulocyte colony-stimulating factor mobilizes dormant hematopoietic stem cells without proliferation in mice. *Blood* **129**, 1901–1912 (2017).
27. Matsumoto, A. et al. p57 is required for quiescence and maintenance of adult hematopoietic stem cells. *Cell Stem Cell* **9**, 262–271 (2011).
28. Matsuoka, S. et al. Fbxw7 acts as a critical fail-safe against premature loss of hematopoietic stem cells and development of T-ALL. *Genes Dev.* **22**, 986–991 (2008).
29. Morita, Y., Ema, H. & Nakauchi, H. Heterogeneity and hierarchy within the most primitive hematopoietic stem cell compartment. *J. Exp. Med.* **207**, 1173–1182 (2010).
30. Shin, J. Y., Hu, W., Naramura, M. & Park, C. Y. High c-Kit expression identifies hematopoietic stem cells with impaired self-renewal and megakaryocytic bias. *J. Exp. Med.* **211**, 217–231 (2014).
31. Thompson, B. J. et al. Control of hematopoietic stem cell quiescence by the E3 ubiquitin ligase Fbw7. *J. Exp. Med.* **205**, 1395–1408 (2008).
32. Zou, P. et al. $p57^{Kip2}$ and $p27^{Kip1}$ cooperate to maintain hematopoietic stem cell quiescence through interactions with Hsc70. *Cell Stem Cell* **9**, 247–261 (2011).
33. Mahajan, M. M. et al. A quantitative assessment of the content of hematopoietic stem cells in mouse and human endosteal-bone marrow: a simple and rapid method for the isolation of mouse central bone marrow. *BMC Hematol.* **15**, 9 (2015).
34. Busch, K. et al. Fundamental properties of unperturbed haematopoiesis from stem cells in vivo. *Nature* **518**, 542–546 (2015).
35. Fanti, A. K. et al. Flt3- and Tie2-Cre tracing identifies regeneration in sepsis from multipotent progenitors but not hematopoietic stem cells. *Cell Stem Cell* **30**, 207–218 (2023).
36. Schoedel, K. B. et al. The bulk of the hematopoietic stem cell population is dispensable for murine steady-state and stress hematopoiesis. *Blood* **128**, 2285–2296 (2016).
37. Sun, J. et al. Clonal dynamics of native haematopoiesis. *Nature* **514**, 322–327 (2014).
38. Yokomizo, T. et al. Independent origins of fetal liver haematopoietic stem and progenitor cells. *Nature* **609**, 779–784 (2022).
39. Challen, G. A., Pietras, E. M., Wallscheid, N. C. & Signer, R. A. J. Simplified murine multipotent progenitor isolation scheme: establishing a consensus approach for multipotent progenitor identification. *Exp. Hematol.* **104**, 55–63 (2021).
40. Wilkinson, A. C. et al. Long-term ex vivo haematopoietic-stem-cell expansion allows nonconditioned transplantation. *Nature* **571**, 117–121 (2019).
41. Decker, M., Leslie, J., Liu, Q. & Ding, L. Hepatic thrombopoietin is required for bone marrow hematopoietic stem cell maintenance. *Science* **360**, 106–110 (2018).
42. O'Neill, A. et al. Thrombopoietin maintains cell numbers of hematopoietic stem and progenitor cells with megakaryopoietic potential. *Haematologica* **106**, 1883–1891 (2021).
43. de Graaf, C. A. et al. Regulation of hematopoietic stem cells by their mature progeny. *Proc. Natl Acad. Sci. USA* **107**, 21689–21694 (2010).
44. Kreso, A. & Dick, J. E. Evolution of the cancer stem cell model. *Cell Stem Cell* **14**, 275–291 (2014).
45. Stauber, J., Greally, J. M. & Steidl, U. Preleukemic and leukemic evolution at the stem cell level. *Blood* **137**, 1013–1018 (2021).
46. Flores-Figueroa, E., Varma, S., Montgomery, K., Greenberg, P. L. & Gratzinger, D. Distinctive contact between CD34+ hematopoietic progenitors and CXCL12+CD271+ mesenchymal stromal cells in benign and myelodysplastic bone marrow. *Lab Invest.* **92**, 1330–1341 (2012).
47. Hanoun, M. et al. Acute myelogenous leukemia-induced sympathetic neuropathy promotes malignancy in an altered hematopoietic stem cell niche. *Cell Stem Cell* **15**, 365–375 (2014).

Methods

Mice

B6.Cg-Gt(ROSA)26Sor$^{tm14(CAG-tdTomato)/Hze}$*/J* (iTdTomato) (007914), C57BL/6J (CD45.2) (000664) and *B6.SJL-Ptprc*^{a} *Pepc*^{b}*/BoyJ* (CD45.1) (002014) mice were purchased from The Jackson Laboratory. Nestin–GFP mice[48] were bred in our facility. *Cdh5-creER*, *Cdh2-creER*, *Cxcl12*$^{fl/fl}$, *Kitl*$^{fl/fl}$, *Tpo*$^{-/-}$ and Tg(Alb-Tpo) mice were provided by R. H. Adams, L. Li, T. Nagasawa, S. J. Morrison, F. J. de Sauvage and W. S. Alexander, respectively. Unless indicated otherwise, 8–10-week-old mice of both sexes were used for experiments. All these mice were backcrossed with C57BL/6J mice for more than ten generations and maintained in pathogen-free conditions under a 12 h–12 h light–dark cycle, at a temperature of 21 ± 1 °C and humidity of 40–70%, and were fed with autoclaved food and water. This study complied with all ethical regulations involving experiments with mice, and all experimental procedures performed on mice were approved by the Institutional Animal Care and Use Committee of Albert Einstein College of Medicine. No randomization or blinding was used to allocate experimental groups.

Femoral bone transplantation

Femurs with intact periosteum were isolated from 8–10-week-old donor mice and preserved on ice in PBS (21-040-CV, Corning) until they were implanted in recipient mice. For transplantation of a single femur, non-conditioned recipient mice that were age and sex-matched with donor mice were anaesthetized with ketamine and xylazine, and a small incision was made at their unilateral thoracic region. Subsequently, the preserved femur was implanted subcutaneously, and the wound was closed. For transplantation of six femurs, small incisions were made at the bilateral cervical, thoracic and pelvic regions of recipient mice, and then one femur was implanted in each area, followed by wound closure. A sham operation was performed by making small incisions on the same area of skin as the control bone transplantation group and closing them.

Parabiosis

Parabionts were generated by making an incision in the skin from the elbow to the knee of mice on opposite sides of each mouse. The elbows and knees were paired together by s.c. suturing. The skin was then matched from one mouse to the other, sutured together and secured with wound clips.

Splenectomy

After mice were anaesthetized with ketamine and xylazine, a longitudinal incision was made in the skin and peritoneum on the left dorsolateral side of the abdomen, caudal to the last rib. The splenic artery was ligated and the spleen was removed. The abdominal wall was then closed, and the skin was sutured. A sham operation was performed by exteriorizing the spleen and then reinserting it into the abdominal cavity.

In vivo treatment

For G-CSF treatment, G-CSF (NEUPOGEN/Filgrastim; 300 μg ml^{-1}, purchased from Jack D. Weiler Hospital of Albert Einstein College of Medicine) was injected s.c. at a dose of 125 μg kg^{-1} twice a day (eight divided doses) beginning in the evening of the first day. When used in bone transplantation experiments, G-CSF was administered to all groups at 1 month after the femurs were implanted or a sham operation was performed unless otherwise indicated. When HSC mobilization was checked, blood was collected at 3 h or 7 days after the final morning dose. For induction of CreER-mediated recombination, 8–10-week-old *Cdh5-creER;iTdTomato* mice were injected intraperitoneally with 2 mg tamoxifen (T5648, Sigma-Aldrich) dissolved in corn oil (C8267, Sigma-Aldrich) for five consecutive days (10 mg in total per mouse). Then, 4 weeks after the injection, these mice were used as hosts, or their femurs were isolated for transplantation. In experiments examining the overlap of *Cdh2*$^{+}$ cells and MSCs, 8–10-week-old *Cdh2-creER;iTdTomato* or *Cdh2-creER;iTdTomato;Nestin-GFP* mice were injected with tamoxifen and subjected to analyses 4 weeks after the injection. In experiments using *Cdh2-creER;Cxcl12*$^{fl/fl}$ or *Cxcl12*$^{fl/fl}$ mice as hosts, tamoxifen was administered at 2 months after the femurs were implanted or a sham operation was performed in these mice. In parabiosis experiments, each mouse of the parabionts was injected with 2 mg tamoxifen for five consecutive days (20 mg in total per parabiont) 3 weeks after the surgery. Then, 4 weeks after the injection, the parabionts were subjected to analyses. In experiments using *Cdh2-creER;Kitl*$^{fl/fl}$ or *Kitl*$^{fl/fl}$ mice as hosts, tamoxifen was administered to four to five-week-old mice before femurs were implanted or a sham operation was performed.

Whole-mount imaging of host femurs and femoral grafts

Antibodies used for immunofluorescence staining of femoral grafts and host femurs are CD31 (PECAM1) Alexa Fluor 647 (MEC13.3, 102516) and CD144 (VE-cadherin) Alexa Fluor 647 (BV13, 138006) from BioLegend. For all imaging experiments, these antibodies (5 μg each) were injected into mice through the retro-orbital plexus for the vasculature staining, and mice were euthanized 10 min after injection. Femoral grafts and host femurs were then isolated and fixed in 4% paraformaldehyde (PFA; 15710, Electron Microscopy Sciences) overnight at 4 °C. For cryopreservation, the bones were incubated sequentially in 10%, 20% and 30% sucrose/PBS at 4 °C for 1 h each, embedded and flash-frozen in SCEM embedding medium (C-EM002, SECTION-LAB) and stored at −80 °C. For whole-mount imaging, bones were placed at −20 °C overnight and shaved with a Cryostat (CM3050, Leica) until the BM cavity was fully exposed. The sections were carefully collected from the melting embedding medium, rinsed with PBS and post-fixed with 4% cold PFA for 10 min followed by permeabilization in 0.5% Triton X-100/PBS for 3 h at room temperature (20–25 °C) and incubation with 2 μg ml^{-1} 4′,6-diamino-2-phenylindole (DAPI; D9542, Sigma-Aldrich) for 30 min. Images were acquired at room temperature using the Zeiss Axio examiner D1 microscope (Zeiss) with a confocal scanner unit (Yokogawa), and reconstructed in three dimensions with SlideBook 6 (Intelligent Imaging Innovations), Photoshop 26 (Adobe) and Fiji build of ImageJ 2 (National Institute of Health, NIH) software.

Cell preparation

For analyses of haematopoietic cells in host femurs and femoral grafts, BM cells in these bones were flushed and dissociated using a 1 ml syringe with PBS through a 21-gauge needle. For analyses of haematopoietic cells throughout the mouse body, BM cells in endogenous and grafted femurs, tibias, humeri and pelvis were collected by flushing and dissociating, and radii, skull, spine, sternum and ribs were minced into small pieces with scissors, crushed with a mortar and pestle and filtered through a 70 μm cell strainer. Splenic cells were obtained by gentle grinding with slide glasses and passing through a 70 μm cell strainer. Cells in the liver were obtained by gentle grinding with slide glasses followed by digestion at 37 °C for 30 min in 1 mg ml^{-1} collagenase type IV (17104019, Gibco), 2 mg ml^{-1} dispase (17105041, Gibco) and 50 μg ml^{-1} DNase I (DN25, Sigma-Aldrich). Peripheral blood was collected by retro-orbital bleeding of mice anaesthetized with isoflurane and mixed with EDTA to prevent clotting. The data from the bones above, spleen, liver and blood (assumed to be 2 ml per animal) were summed to determine the total HSC numbers in the mouse body. For analyses of BM stromal cells, intact flushed BM plugs were digested at 37 °C for 30 min in 1 mg ml^{-1} collagenase type IV, 2 mg ml^{-1} dispase and 50 μg ml^{-1} DNase I in Hank's balanced salt solution with calcium and magnesium (21-023-CV, Gibco). These single-cell suspensions were then subjected to red blood cell lysis with ammonium chloride and washed in ice-cold PEB (PBS containing 0.5% BSA and 2 mM EDTA).

Flow cytometry analysis and cell sorting

Cells were surface-stained in PEB for 30–60 min at 4 °C. Antibodies used for flow cytometry analyses and sorting were as follows: anti-CD45

APC-eFluor 780 (30-F11, 47-0451-82), anti-TER-119 APC-eFluor 780 (TER-119, 45-5921-82), anti-CD31 PE-Cyanine7 (390, 25-0311-82), anti-CD51 biotin (RMV-7, 13-0512-85), anti-CD140a (PDGFRA) PE (APA5, 12-1401-81), anti-CD140a PE-Cyanine7 (APA5, 25-1401-81), anti-Ly6A/E (SCA-1) FITC (D7, 11-5981-82), anti-Ly6G/Ly6C (GR-1) FITC (RB6-8C5, 11-5931-85), anti-Ly6G/Ly6C APC-eFluor 780 (RB6-8C5, 47-5931-82), anti-CD11b PE (M1/70, 12-0112-83), anti-CD11b PE-Cyanine7 (M1/70, 25-0112-82), anti-CD11b APC-eFluor 780 (M1/70, 47-0112-82), anti-B220 APC-eFluor 780 (RA3-6B2, 47-0452-82), anti-CD3e APC-eFluor 780 (145-2C11, 47-0031-82), anti-CD48 PerCP-eFluor 710 (HM48-1, 46-0481-85), anti-CD48 PE-Cyanine7 (HM48-1, 25-0481-80), anti-CD41 PerCP-eFluor 710 (MWReg30, 46-0411-82), anti-CD34 eFluor 660 (RAM34, 50-0341-82, 1:50 dilution), anti-CD135 (FLT3) PerCP-eFluor 710 (A2F10, 46-1351-82), anti-CD115 APC (AFS98, 17-1152-82) and anti-CD45.1 PE-Cyanine7 (A20, 25-0453-82) from eBioscience; anti-CD62E PE (10E9.6, 553751) from BD Biosciences; anti-KIT PE-Cyanine7 (2B8, 105814), anti-CD117 Brilliant Violet 421 (2B8, 105828), anti-CD150 PE (TC15-12F12.2, 115904), F4/80 PE (BM8, 123110) and anti-CD45.2 APC (104, 109814) from BioLegend; and anti-CD3e PerCP-Cyanine5.5 (145-2C11, 65-0031-U100) from Tonbo Biosciences. Streptavidin FITC (11-4317-87) and Streptavidin PerCP-eFluor 710 (46-4317-82) were purchased from eBioscience. Unless otherwise specified, all antibodies, Streptavidin FITC and Streptavidin PerCP-eFluor 710 were used at a 1:100 dilution. Flow cytometry analyses were carried out on the BD LSRII (BD Biosciences) system, and cell sorting experiments were performed using BD FACSAria (BD Biosciences). Dead cells and debris were excluded by forward scatter, side scatter and DAPI staining (1 μg ml^{-1}) profiles. Data were analysed using FACS Diva 6.1 (BD Biosciences) and FlowJo 10 software. Gating strategies are shown in Supplementary Fig. 1.

Cell cycle analysis

Single-cell suspensions were stained for cell surface markers, and subsequently fixed and permeabilized with BD Cytofix/Cytoperm solution (554714, BD Biosciences) according to the manufacturer's instructions. The cells were then stained with DAPI (Sigma-Aldrich) at 5 μg ml^{-1} and anti-Ki-67 PerCP eFluor 710 antibody (SolA15, 46-5698-80, eBioscience) or anti-Ki-67 eFluor 660 antibody (SolA15, 50-5698-82, eBioscience) at 1:100 dilution for 30 min at 4 °C. After washing, the cells were analysed on the BD LSRII (BD Biosciences) system. A $DAPI^{low}Ki\text{-}67^{low}$ fraction was designated as the G0 phase of the cell cycle.

Blood cell analysis

Peripheral blood was diluted in PBS, and blood parameters were determined with the Advia120 Hematology System (Siemens).

Competitive BM and HSC transplantation

Competitive repopulation assays were performed using the CD45.1/CD45.2 congenic system. CD45.1 recipient mice were lethally irradiated (12 Gy, two split doses at least three hours apart) in a caesium mark 1 irradiator (JL Shepherd & Associates). For BM repopulation assays, 1×10^6 CD45.2 donor-nucleated BM cells were transplanted into irradiated recipients together with 1×10^6 CD45.1 BM cells. For HSC repopulating assays, 200 HSCs (CD45.2) were sorted from BM cells and transplanted into irradiated CD45.1 recipients together with CD45.1 competitor BM cells calculated to contain 200 HSCs (1:1 HSC ratio). For secondary BMT, 3×10^6 BM cells from primary recipient mice were transplanted into newly irradiated (12 Gy) CD45.1 recipients. CD45.1/CD45.2 chimerism of the myeloid ($CD11b^+$), B ($B220^+$) and T ($CD3\varepsilon^+$) lineages in recipient blood was analysed up to 5 months after BM or HSC transplantation using a flow cytometer, and that of BM cells was checked at 5 months after BM or HSC transplantation, at which the mice were euthanized.

Ex vivo HSC culture

Ex vivo HSC cultures were performed using F12-PVA-based culture conditions as previously described[40]. In brief, HSCs were sorted into 96-well flat-bottom plates containing 200 μl HSC medium and expanded at 37 °C with 5% CO_2 for up to 28 days. Medium changes were made every 2–3 days. Cells were split at a 1:3 ratio into new plates when reaching 80–90% confluency. After expansion, the cells were used for non-conditioned transplantation.

Non-conditioned HSPC transplantation

HSCs were purified from CD45.2 mice and expanded, as described above. Expanded HSPCs (10^6 LSK cells per recipient mouse) were then transferred into non-irradiated tamoxifen-administered *Cdh2-creER;Kitl*$^{fl/fl}$ mice (backcrossed with CD45.2 mice for more than 10 generations) after the transplantation of one or six WT femurs, split into three doses over consecutive days.

Targeted limb irradiation

Animals were anaesthetized by isoflurane before irradiation using the Small Animal Radiation Research Platform, SARRP (XStrahl). The orthovoltage X-ray unit operates at 220 kVp and 13 mA. Before irradiation, a static X-ray scan was acquired using 50 kVp and 0.7 mA tube current with Al filtration. Mice were maintained in a circular lucite jig with whole-body lead shielding (to protect the individualized compartments from unwanted irradiation) and ports through which secured four limbs protruded and were irradiated to 20 Gy in a single fraction.

RNA extraction and RT–qPCR analysis

A total of 2×10^3 MSCs or HSCs were sorted directly into lysis buffer and stored at −80 °C. mRNA was extracted using the Dynabeads mRNA DIRECT Purification Kit (61012, Invitrogen) according to the manufacturer's protocols. Conventional reverse transcription (RT) with random hexanucleotide primers was then performed using the RNA to cDNA EcoDry Premix (639549, TaKaRa) in accordance with the manufacturer's instructions. Quantitative PCR (qPCR) was performed in 384-well plates with FastStart Universal SYBR Green Master Mix (04913914001, Roche) on the QuantStudio 6 Flex Real-Time PCR System v.1.7.2 (Applied Biosystems). The PCR protocol started with one cycle at 95 °C (10 min) and continued with 40 cycles at 95 °C (15 s) and 60 °C (1 min). All mRNA abundance was calculated relative to the corresponding amount of *Actb* (encoding β-actin) using the ΔC_t method. A list of the primer sequences is provided in Supplementary Table 1.

ELISA

For analysis of BMEF, the BM of one femur or pelvis was flushed out using 1 ml of PBS, and the cells were subsequently pelleted by centrifugation. The resulting supernatant was transferred to another tube and stored at −80 °C until analysis. For analysis of serum, blood was allowed to clot at room temperature, and serum was separated by centrifugation and stored at −80 °C until analysis. Cytokine levels in BMEF and serum were then measured using mouse IL-1β (BMS6002), IL-6 (KMC0061) ELISA kits (Thermo Fisher Scientific) and TNF (MTA00B-1), CXCL12/SDF-1α (MCX120), SCF (MCK00) and TPO (MTP00) Quantikine ELISA kits (R&D Systems) according to the manufacturer's protocols.

Statistics and reproducibility

All data are presented as mean ± s.e.m. *n* represents the number of mice in each experiment, as detailed in the figure legends, and experiments presented were successfully reproduced in at least three biological replicates. No statistical method was used to predetermine sample sizes, and sample sizes were determined by previous experience with similar models of haematopoiesis, as shown in previous experiments performed in our laboratory[13,14,16,19,20,47]. Sample exclusion was only done as a result of premature mouse death. Statistical significance was determined by an unpaired, two-tailed Student's *t*-test to compare two groups or a one-way ANOVA with Tukey's multiple-comparison tests for multiple group comparisons. Data presentation and statistical analyses were performed using Prism 10 (GraphPad), Excel 16 (Microsoft),

SlideBook 6 (Intelligent Imaging Innovations), Photoshop 26 (Adobe) and FlowJo 10 software.

The data in Fig. 2j,k were obtained in the same experiments, and data from the sham-operated mice were reused in each of these figure panels. The data in Extended Data Fig. 7b,c were obtained in the same experiments, and data from the sham-operated mice were reused in each of these figure panels. The data in Extended Data Fig. 8i,j were obtained in the same experiments, and data from the sham-operated *Cxcl12*$^{fl/fl}$ and *Cdh2-creER;Cxcl12*$^{fl/fl}$ mice were reused in each of these figure panels. The data in Fig. 3h,i were obtained in the same experiments, and data from the sham-operated *Cxcl12*$^{fl/fl}$ and *Cdh2-creER;Cxcl12*$^{fl/fl}$ mice were reused in each of these figure panels. The data in Fig. 4c,d were obtained in the same experiments, and data from the sham-operated *Kitl*$^{fl/fl}$ and *Cdh2-creER;Kitl*$^{fl/fl}$ mice were reused in each of these figure panels. The data in Fig. 5c,d were obtained in the same experiments, and data from the sham-operated *Tpo*$^{+/+}$, *Tpo*$^{+/-}$ and *Tpo*$^{-/-}$ mice were reused in each of these figure panels. The data in Fig. 5h,i were obtained in the same experiments, and data from the sham-operated WT and *Tpo*-Tg mice were reused in each of these figure panels.

Reporting summary

Further information on research design is available in the Nature Portfolio Reporting Summary linked to this article.

Data availability

Source data are provided with this paper.

48. Mignone, J. L., Kukekov, V., Chiang, A. S., Steindler, D. & Enikolopov, G. Neural stem and progenitor cells in nestin-GFP transgenic mice. *J. Comp. Neurol.* **469**, 311–324 (2004).

Acknowledgements We dedicate this achievement to P. S. Frenette, who conceived and initially supervised the study but unfortunately passed away in July 2021. We will forever be indebted to him for his brilliant mentorship and leadership. His rigorous approach and unparalleled enthusiasm for science, especially for this project aiming to answer a long-standing question in the stem cell field, laid the foundation for this Article. He will be deeply missed by all, and his passion for science will be carried on by his mentees and colleagues. We thank R. H. Adams, L. Li, T. Nagasawa, S. J. Morrison, F. J. de Sauvage and W. S. Alexander for providing *Cdh5-creER*, *Cdh2-creER*, *Cxcl12*$^{fl/fl}$, *Kitl*$^{fl/fl}$, *Tpo*$^{-/-}$ and Tg(Alb-Tpo) mice, respectively; N. Asada, F. Nakahara, T. Mizoguchi and S. Pinho for advice with the initial experiments; C. Prophete, P. Ciero, C. D. Cruz, A. Landeros, G. Amatuni, J. Kazmi and M. Bhuiyan for technical assistance; L. Tesfa for assistance in cell sorting; N. P. Brodin for the targeted limb irradiation experiments; and the members of the Frenette and Steidl laboratories, B. Will, A. Skoultchi and T. Shichita for discussions and advice. This work was supported by grants from the NIH (R01DK056638 to P.S.F. and K.G., R01DK112976, R01HL116340 and U01DK116312 to P.S.F., R01DK130895 to K.G., R35CA253127, R01HL157948 and P01CA285250 to U.S.), the New York State Department of Health NYSTEM IIRP (C029154 and C029570 to P.S.F.) and the Montefiore Einstein Comprehensive Cancer Center core support grant (P30CA013330). S.T. was supported by the Japan Society for the Promotion of Science (JSPS) Postdoctoral Fellowship for Research Abroad, the Uehara Memorial Foundation Research Fellowship and the NYSTEM Empire State Institutional Program in Stem Cell Research. T.M. was supported by the Fondation ARC pour la Recherche sur le Cancer, the Association pour le Développement de l'Hématologie Oncologie (ADHO), the Société Française d'Hématologie and the Philip foundation. D.K.B. was supported by Individual Predoctoral National Research Service Award (F30HL154749), Training Program in Cellular and Molecular Biology and Genetics (5T32GM007491) and Medical Scientist Training Program (5T32GM007288) from NIH and by the NYSTEM Empire State Institutional Program in Stem Cell Research. K.G. was supported by the Betty & Sheldon Feinberg Senior Faculty Scholar in Cancer Research fund and by a pilot project fund from the Cancer Dormancy Institute of the Montefiore Einstein Comprehensive Cancer Center. U.S. holds the Edward P. Evans Endowed Professorship in Myelodysplastic Syndromes at Albert Einstein College of Medicine, which was supported by a grant from the Edward P. Evans Foundation. This work was also supported by J. A. and Myles P. Dempsey. Some panels in Figs. 1–5 and Extended Data Figs. 1–4, 6 and 8–10 include illustrations created using BioRender.

Author contributions S.T. conceived the project, designed the study, performed most of the experiments, analysed and interpreted the data, and wrote the manuscript. T.M., D.K.B. and C.X. helped with experiments. W.R.K. performed the targeted limb irradiation, and C.G. provided input on its experimental design. A.B. advised on the study. P.S.F. supervised and funded the project, analysed and interpreted the data and commented on the figure plan. K.G. and U.S. supervised and funded the study, analysed and interpreted the data, and edited the manuscript. All of the authors discussed the results and reviewed the manuscript.

Competing interests T.M. serves as a consultant for Astellas, Jazz Pharmaceuticals, Servier and Sobi, and has received personal fees from Jazz Pharmaceuticals and Servier outside the submitted work. C.G. has received grants and personal fees from Janssen and Varian, and grants from Celldex outside the submitted work. P.S.F. served as a consultant for Pfizer, received research funding from Ironwood Pharmaceuticals outside the submitted work, and was a shareholder of Cygnal Therapeutics. K.G. has received research funding from ADC Therapeutics and iOnctura outside the submitted work. U.S. has received grants from GlaxoSmithKline, Bayer Healthcare, Aileron Therapeutics and Novartis, and personal fees from GlaxoSmithKline, Bayer Healthcare, Celgene, Aileron Therapeutics, Stelexis Therapeutics, Pieris Pharmaceuticals, Trillium and Pfizer outside the submitted work. U.S. has equity ownership in and has served on the board of directors of Stelexis Therapeutics outside the submitted work. U.S. has equity ownership in Roshon Therapeutics outside the submitted work. The other authors declare no competing interests.

Additional information

Supplementary information The online version contains supplementary material available at https://doi.org/10.1038/s41586-025-09462-5.

Correspondence and requests for materials should be addressed to Shoichiro Takeishi or Ulrich Steidl.

Peer review information *Nature* thanks Iannis Aifantis, Thomas Hoefer and the other, anonymous, reviewer(s) for their contribution to the peer review of this work.

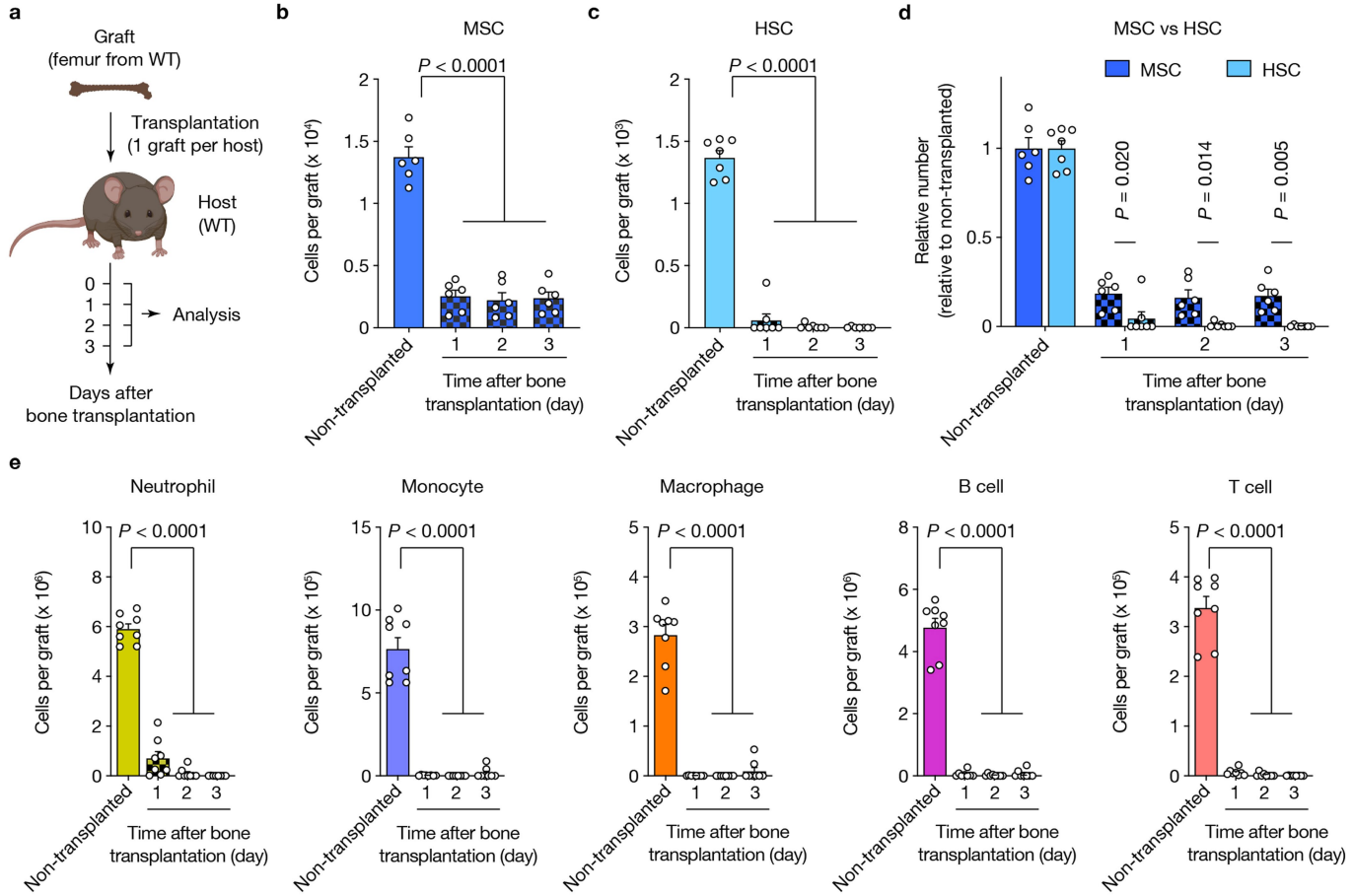

Extended Data Fig. 1 | While MSCs survive in the femoral grafts, virtually no haematopoietic cells are detected shortly after bone transplantation. **a**, Experimental strategy to determine the number of MSCs, HSCs and differentiated haematopoietic cells in the grafts shortly after bone transplantation from WT to WT mice. The diagram was created using BioRender. Takeishi, S. (2025) https://BioRender.com/9d3nv16. **b**, **c**, The number of MSCs (**b**) and HSCs (**c**) in the grafts at the indicated timepoints after bone transplantation. $n = 6, 7$ grafts from 6, 7 host mice, respectively, at each timepoint. **d**, Relative number of MSCs and HSCs in the grafts compared with non-transplanted femurs at the indicated timepoints after bone transplantation. $n = 6, 7$ grafts from 6, 7 host mice, respectively, at each timepoint. **e**, The number of differentiated haematopoietic cells in the grafts at the indicated timepoints after bone transplantation. $n = 8$ grafts from 8 host mice at each timepoint. Data are mean ± s.e.m. Significance was assessed using a two-tailed unpaired Student's *t*-test (**d**) or one-way ANOVA (**b**, **c**, **e**).

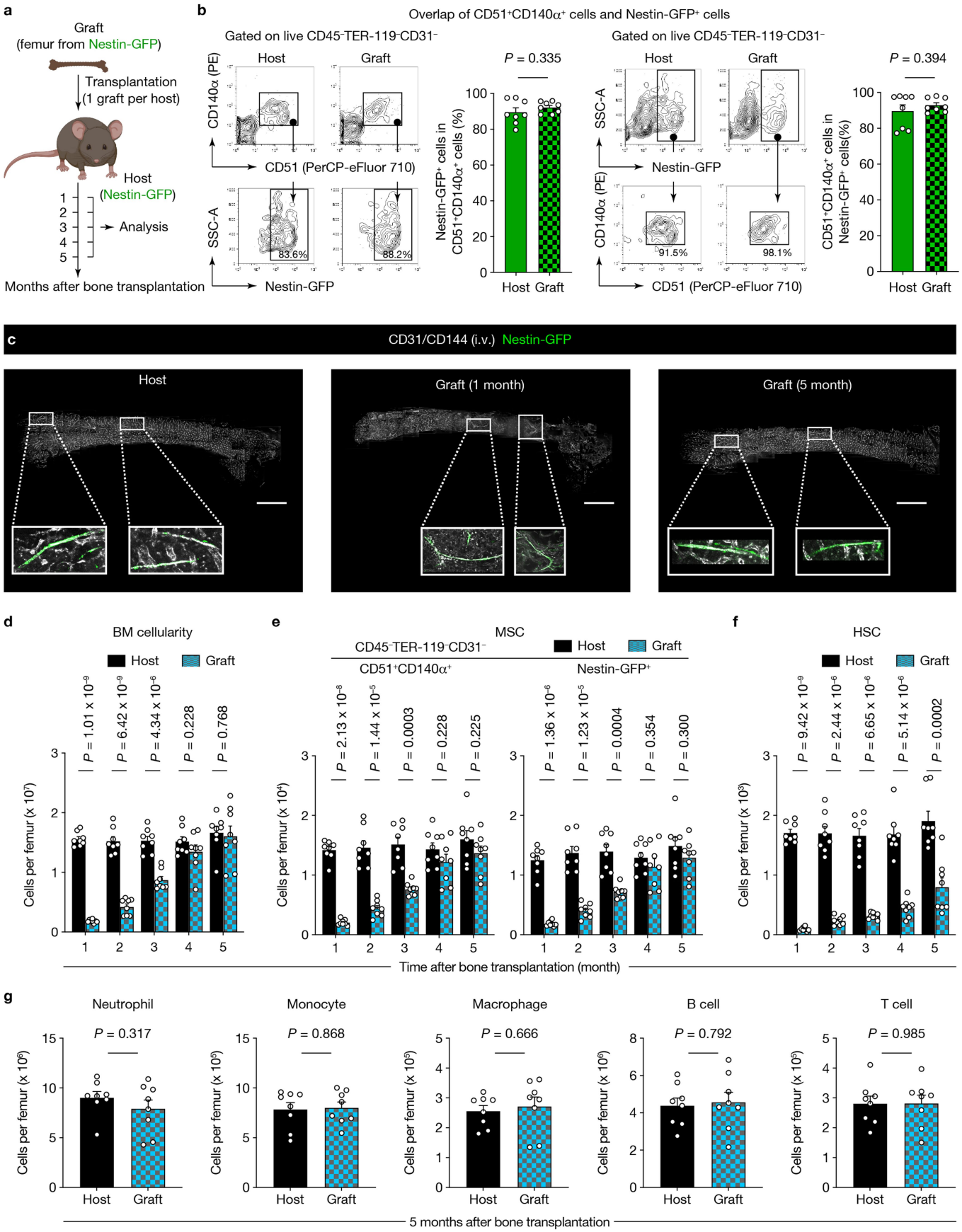

Extended Data Fig. 2 | See next page for caption.

Extended Data Fig. 2 | BM stroma regeneration and haematopoietic recovery in the femoral grafts. a, Schematic of the transplantation of Nestin-GFP femurs into Nestin-GFP mice and analyses. The diagram was created using BioRender. Takeishi, S. (2025) https://BioRender.com/9d3nv16. **b**, Representative flow cytometry plots and the quantification of overlap of $CD51^+CD140\alpha^+$ cells and $Nestin\text{-}GFP^+$ cells in $CD45^-TER\text{-}119^-CD31^-$ fraction of the host femurs and the grafts at 5 months after bone transplantation. 8 host femurs and 8 grafts from 8 host mice. **c**, Representative confocal z-stack projection montages of Nestin-GFP (green) host femur and graft stained for $CD31^+CD144^+$ (white) vasculature at 1 or 5 months after bone transplantation. Scale bars, 1000 μm; four independent experiments yielded similar results. **d**-**f**, The number of BM cells (**d**), MSCs (**e**) and HSCs (**f**) per host femur and graft at the indicated timepoints after bone transplantation. 8 host femurs and 8 grafts from 8 host mice at each timepoint. **g**, The number of differentiated haematopoietic cells per host femur and graft. 8 host femurs and 8 grafts from 8 host mice. Data are mean ± s.e.m. Significance was assessed using a two-tailed unpaired Student's *t*-test.

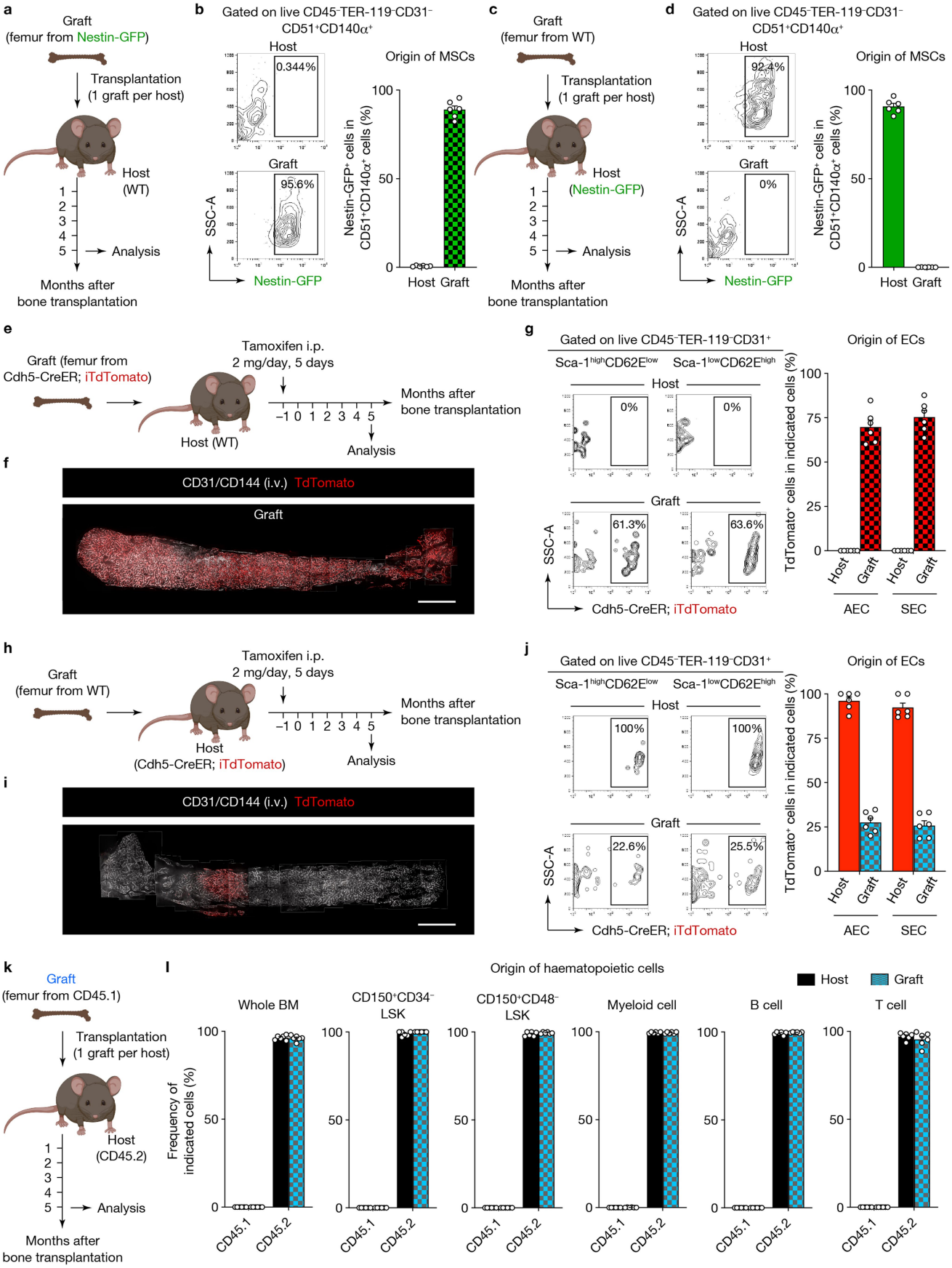

Extended Data Fig. 3 | See next page for caption.

Extended Data Fig. 3 | Determination of the origin of the cells in the femoral grafts. a, Experimental strategy to determine whether MSCs in the grafts are derived from the grafts. **b**, Left: representative flow cytometry plots of Nestin-GFP$^+$ cells in CD45$^-$TER-119$^-$CD31$^-$CD51$^+$CD140α$^+$ MSCs isolated from the host femurs (top) and the grafts (bottom) in the experiment shown in **a**. Right: the frequency of the Nestin-GFP$^+$ population within the CD45$^-$TER-119$^-$CD31$^-$CD51$^+$CD140α$^+$ fraction in the host femurs and the grafts. 6 host femurs and 6 grafts from 6 host mice. **c**, Experimental strategy to determine whether MSCs in the grafts are derived from the hosts. **d**, Left: representative flow cytometry plots of Nestin-GFP$^+$ cells in CD45$^-$TER-119$^-$CD31$^-$CD51$^+$CD140α$^+$ MSCs isolated from the host femurs (top) and the grafts (bottom) in the experiment shown in **c**. Right: the frequency of the Nestin-GFP$^+$ population within the CD45$^-$TER-119$^-$CD31$^-$CD51$^+$CD140α$^+$ fraction in the host femurs and the grafts. 6 host femurs and 6 grafts from 6 host mice. **e**, Experimental strategy to determine whether ECs in the grafts are derived from the grafts. **f**, Confocal z-stack projection of Cdh5-CreER; iTdTomato (red) graft transplanted to WT mice and stained for CD31$^+$CD144$^+$ (white) vasculature. Scale bar, 1000 μm; three independent experiments yielded similar results. **g**, Left: representative flow cytometry plots of TdTomato$^+$ cells in CD45$^-$TER-119$^-$CD31$^+$SCA-1^{high}CD62E^{low} AEC fraction from the host femurs (top left) and the grafts (bottom left) and in CD45$^-$TER-119$^-$CD31$^+$SCA-1^{low}CD62E^{high} SEC fraction from the host femurs (top right) and the grafts (bottom right) in the experiment shown in **e**. Right: the frequency of the TdTomato$^+$ cells in AEC and SEC fractions in the host femurs and the grafts. 6 host femurs and 6 grafts from 6 host mice. **h**, Experimental strategy to determine whether ECs in the grafts are derived from the hosts. **i**, Confocal z-stack projection of WT graft transplanted to Cdh5-CreER; iTdTomato (red) mice and stained for CD31$^+$CD144$^+$ (white) vasculature. Scale bar, 1000 μm; three independent experiments yielded similar results. **j**, Left: representative flow cytometry plots of TdTomato$^+$ cells in CD45$^-$TER-119$^-$CD31$^+$SCA-1^{high}CD62E^{low} AEC fraction from the host femurs (top left) and the grafts (bottom left) and in CD45$^-$TER-119$^-$CD31$^+$SCA-1^{low}CD62E^{high} SEC fraction from the host femurs (top right) and the grafts (bottom right) in the experiment shown in **h**. Right: the frequency of the TdTomato$^+$ cells in AEC and SEC fractions in the host femurs and the grafts. 6 host femurs and 6 grafts from 6 host mice. **k**, Schematic of the determination of the origin of haematopoietic cells in the grafts. **l**, The frequency of CD45.1$^+$ and CD45.2$^+$ cells in the whole BM cells, HSCs and differentiated haematopoietic cells in the host femurs and the grafts. 6 host femurs and 6 grafts from 6 host mice. Data are mean ± s.e.m. The diagrams in **a**, **c**, **e**, **h** and **k** were created using BioRender. Takeishi, S. (2025) https://BioRender.com/9d3nv16.

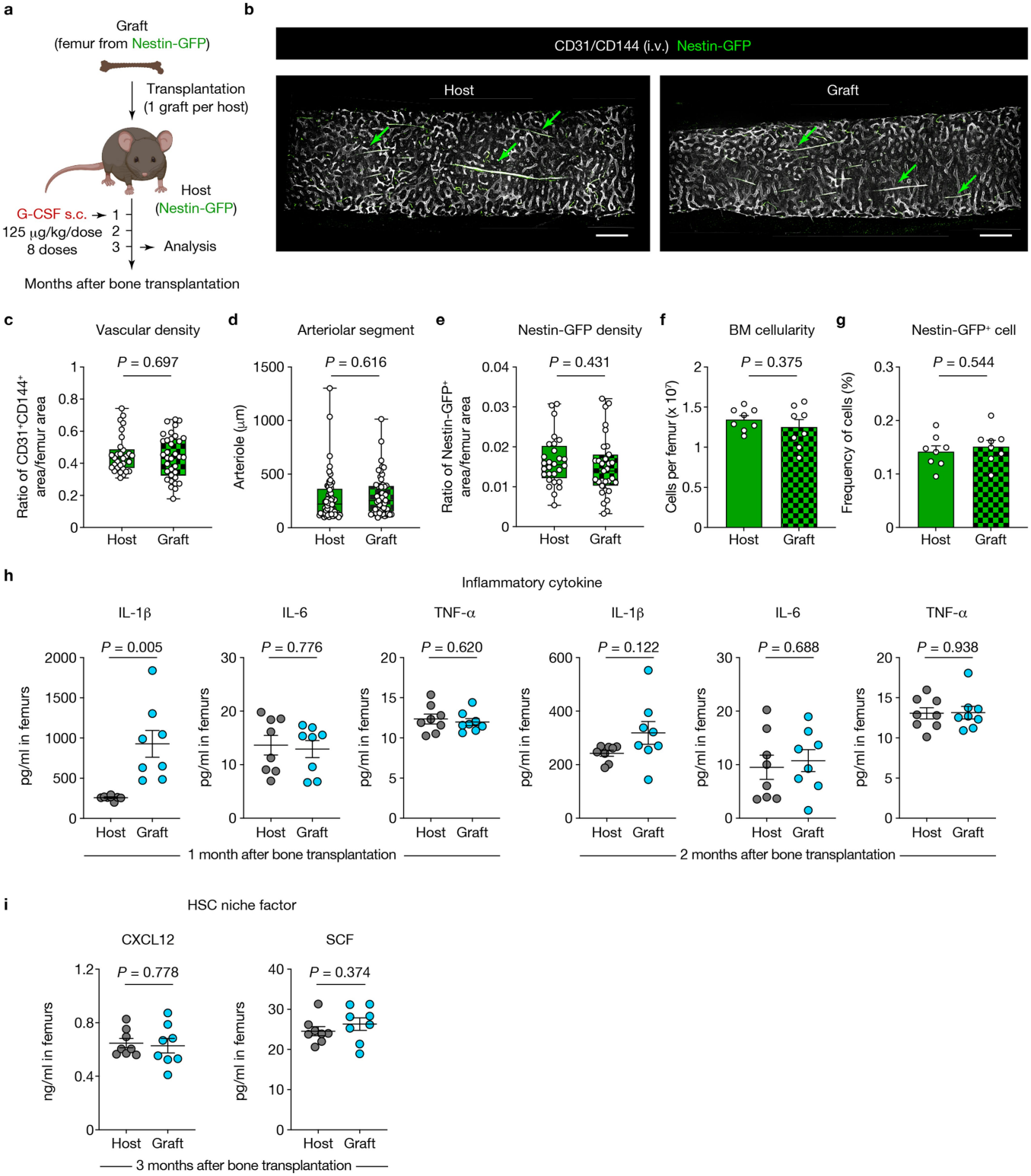

Extended Data Fig. 4 | See next page for caption.

Extended Data Fig. 4 | Normal BM structure and HSC niche function in G-CSF-administered femoral grafts. a, Schematic of the transplantation of Nestin-GFP femurs into Nestin-GFP mice, G-CSF administration and analyses. The diagram was created using BioRender. Takeishi, S. (2025) https://BioRender.com/9d3nv16. **b**, Representative confocal z-stack projection montages of G-CSF-administered Nestin-GFP (green) host femurs and grafts stained for $CD31^+CD144^+$ (white) vasculature. Green arrows indicate arterioles. Scale bars, 100 μm; four independent experiments yielded similar results. **c**, Vasculature density in the host femurs and the grafts, as assessed by quantification of $CD31^+CD144^+$ vascular area divided by total BM area. $n = 30$ and 34 projections in the host femurs and the grafts, respectively; 4 host femurs and 4 grafts from 4 host mice. **d**, Arteriolar segment length in the host femurs and the grafts, as assessed by quantification of the length of the Nestin-GFP^+ signal covering $CD31^+CD144^+$ arterioles. $n = 60$ and 55 projections in the host femurs and the grafts, respectively; 4 host femurs and 4 grafts from 4 host mice. **e**, Nestin-GFP density in the host femurs and the grafts, as assessed by quantification of Nestin-GFP^+ area divided by total BM area. $n = 28$ and 31 projections in the host femurs and the grafts, respectively; 4 host femurs and 4 grafts from 4 host mice. **f**, **g**, BM cellularity (**f**) and the frequency of Nestin-GFP^+ MSCs (**g**) from the host femurs and the grafts, assessed by flow cytometry. 8 host femurs and 8 grafts from 8 host mice. **h**, IL-1β, IL-6 and TNF-α levels in BMEF of the host femurs and the grafts measured by ELISA at the indicated timepoints after bone transplantation in the experiment shown in Fig. 1a. 8 host femurs and 8 grafts from 8 G-CSF-administered host mice. **i**, CXCL12 and SCF levels in BMEF of the host femurs and the grafts measured by ELISA. 8 host femurs and 8 grafts from 8 G-CSF-administered host mice. Data are mean ± s.e.m. For box plots, the box spans from the 25th to 75th percentiles and the centre line is plotted at the median. Whiskers represent the minimum to maximum range. Significance was assessed using a two-tailed unpaired Student's *t*-test.

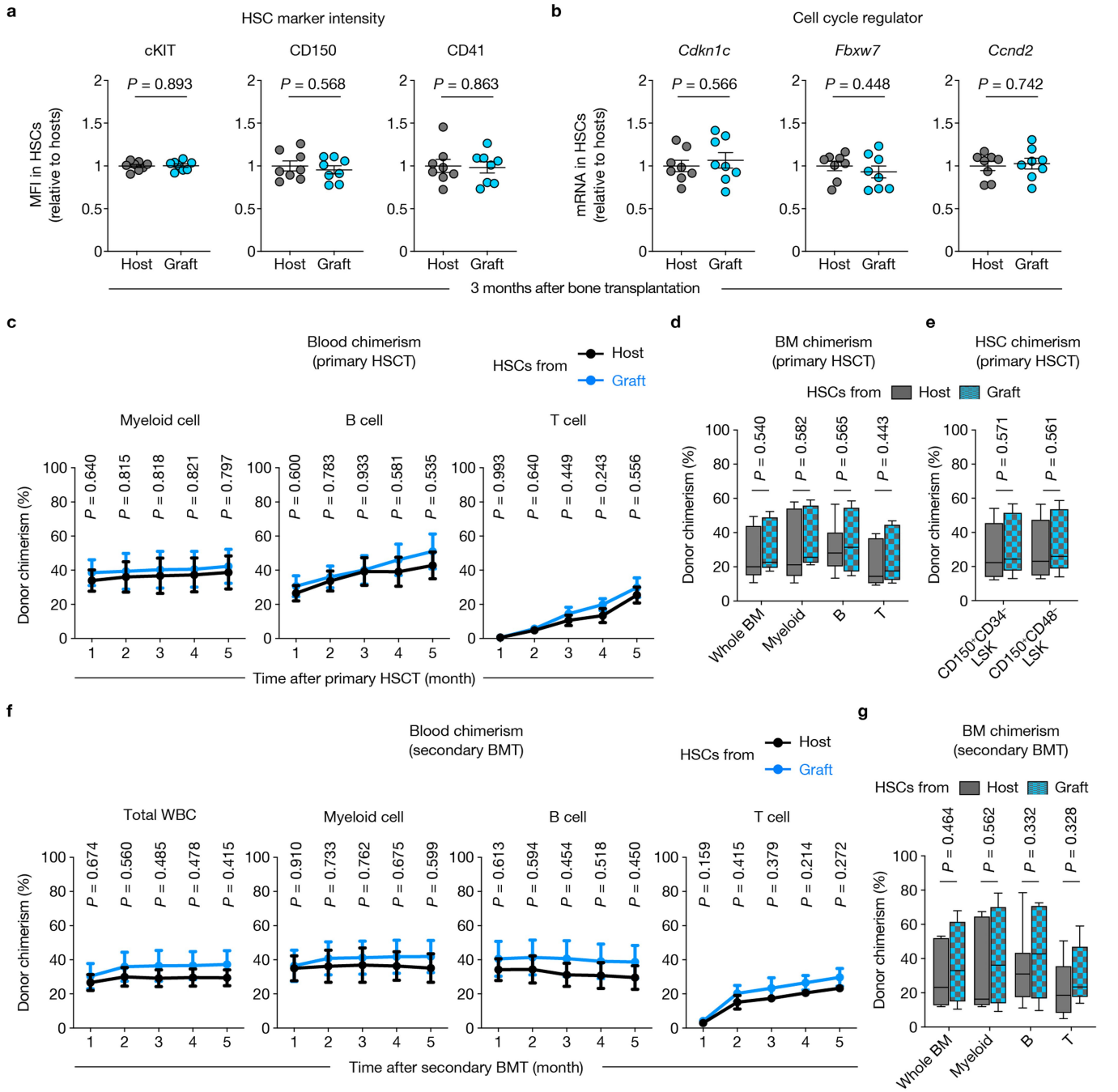

Extended Data Fig. 5 | G-CSF-administered grafts harbour HSCs with normal functions. a, Mean fluorescence intensity (MFI) of cKIT, CD150 and CD41 in HSCs from the host femurs and the grafts in the experiment shown in Fig. 1a. 8 host femurs and 8 grafts from 8 G-CSF-administered host mice. **b**, Quantification of mRNA levels of the indicated cell cycle regulators in HSCs from the host femurs and the grafts. 8 host femurs and 8 grafts from 8 G-CSF-administered host mice. **c**, Blood chimerism (CD45.2) in myeloid ($CD11b^+$), B ($B220^+$) and T ($CD3\varepsilon^+$) cells of recipient mice transplanted with HSCs (CD45.2) from G-CSF-administered host femurs or grafts in competition with $CD45.1^+$ BM cells at the indicated timepoints after primary HSCT in the experiment shown in Fig. 1a. $n = 10$ mice per group. **d**, **e**, BM chimerism in whole BM, myeloid, B, T cells (**d**) and HSCs (**e**) at 5 months after primary HSCT. $n = 10$ mice per group. **f**, Blood chimerism (CD45.2) in total WBC, myeloid, B and T cells of recipient mice at the indicated timepoints after secondary BMT. $n = 10$ mice per group. **g**, BM chimerism in whole BM, myeloid, B and T cells at 5 months after secondary BMT. $n = 10$ mice per group. Data are mean ± s.e.m. For box plots, the box spans from the 25th to 75th percentiles and the centre line is plotted at the median. Whiskers represent the minimum to maximum range. Significance was assessed using a two-tailed unpaired Student's *t*-test.

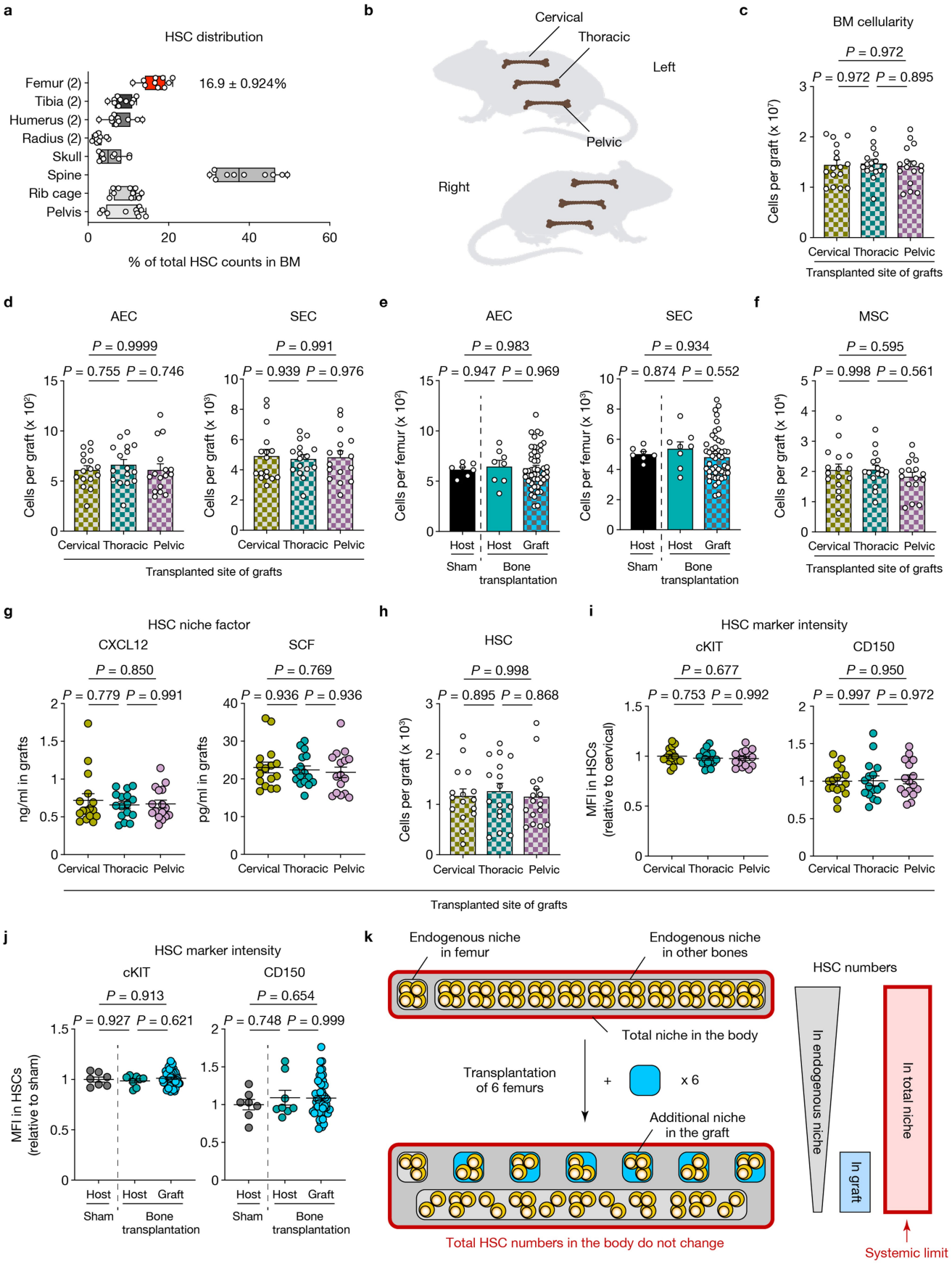

Extended Data Fig. 6 | See next page for caption.

Extended Data Fig. 6 | Characterization of HSCs and their niches in the host femurs and the grafts after six femur transplantation. a, HSC distribution in the mouse BM, as assessed by flow cytometry. The number in parentheses indicates the number of bones examined per mouse. *n* = 10 mice. **b**, Schematic of transplanted sites of femurs in the experiment shown in Fig. 2a. The diagram was created using BioRender. Takeishi, S. (2025) https://BioRender.com/9d3nv16. **c**, **d**, The number of BM cells (**c**) and ECs (**d**) in the grafts by their transplanted site. *n* = 16 grafts per transplanted site. **e**, EC numbers per host femur and graft. 7 femurs from 7 sham-operated mice, 8 host femurs and 48 grafts from 8 bone transplantation hosts. **f**, MSC numbers in the grafts by their transplanted site. *n* = 16 grafts per transplanted site. **g**, CXCL12 and SCF levels in BMEF of the grafts by their transplanted site. *n* = 16 grafts per transplanted site. **h**, HSC numbers in the grafts by their transplanted site. *n* = 16 grafts per transplanted site. **i**, MFI of cKIT and CD150 in HSCs from the grafts by their transplanted site. *n* = 16 grafts per transplanted site. **j**, MFI of cKIT and CD150 in HSCs from the host femurs and the grafts. 7 femurs from 7 sham-operated mice, 8 host femurs and 48 grafts from 8 bone transplantation hosts. **k**, Diagram showing the results of six WT femur transplantation into WT mice. Data are mean ± s.e.m. For box plots, the box spans from the 25th to 75th percentiles and the centre line is plotted at the median. Whiskers represent the minimum to maximum range. Significance was assessed using one-way ANOVA.

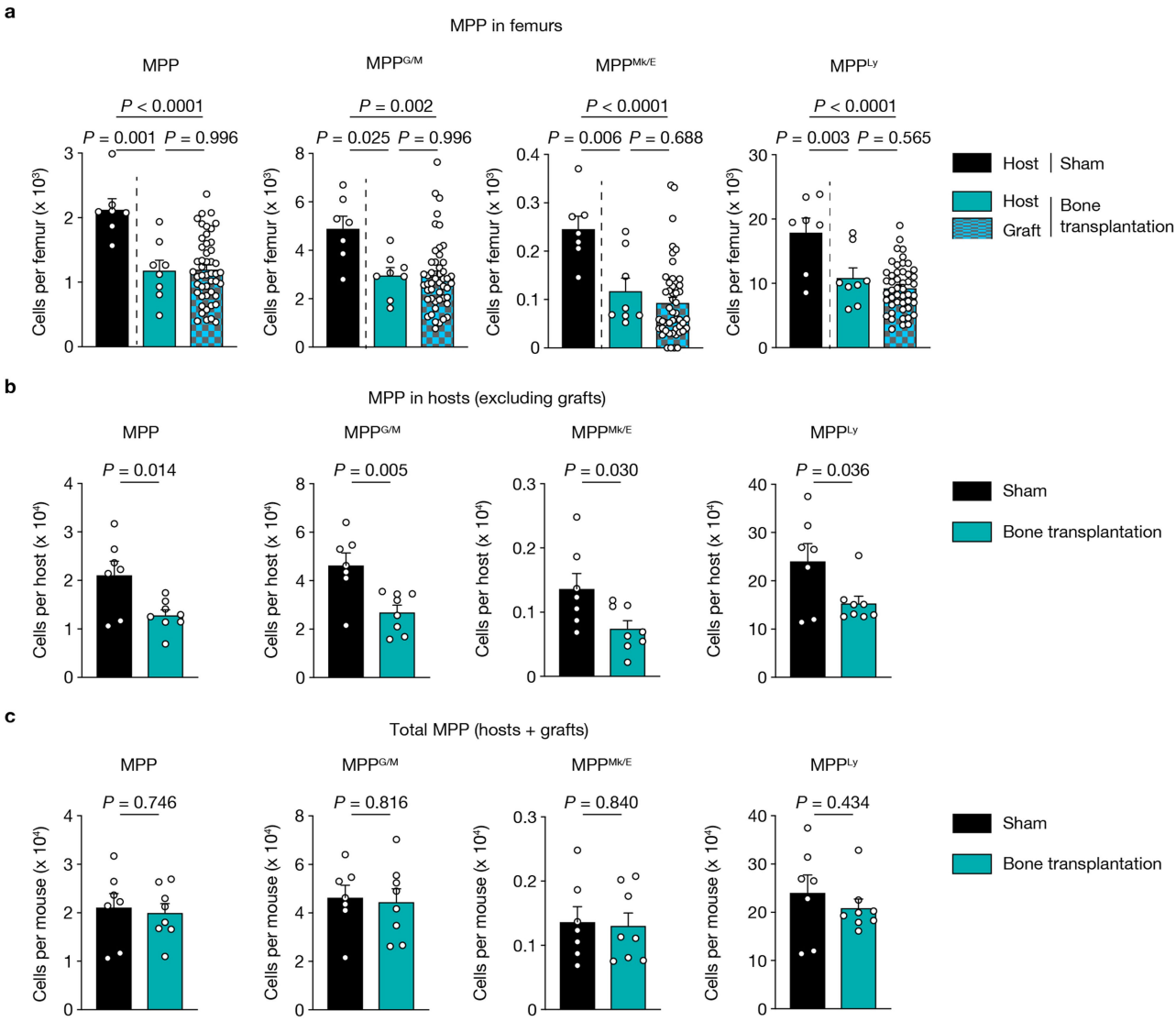

Extended Data Fig. 7 | MPP numbers in the entire body do not alter after transplantation of six WT femurs. a, The number of the indicated MPP subsets per host femur and graft in the experiment shown in Fig. 2a. 7 femurs from 7 sham-operated mice, 8 host femurs and 48 grafts from 8 bone transplantation hosts. **b, c**, The number of the indicated MPP subsets in the entire body of hosts (excluding grafts) (**b**), and the sum of MPPs in the hosts and the grafts (**c**). $n = 7, 8$ mice, respectively. Data are mean ± s.e.m. Significance was assessed using a two-tailed unpaired Student's *t*-test (**b**, **c**) or one-way ANOVA (**a**).

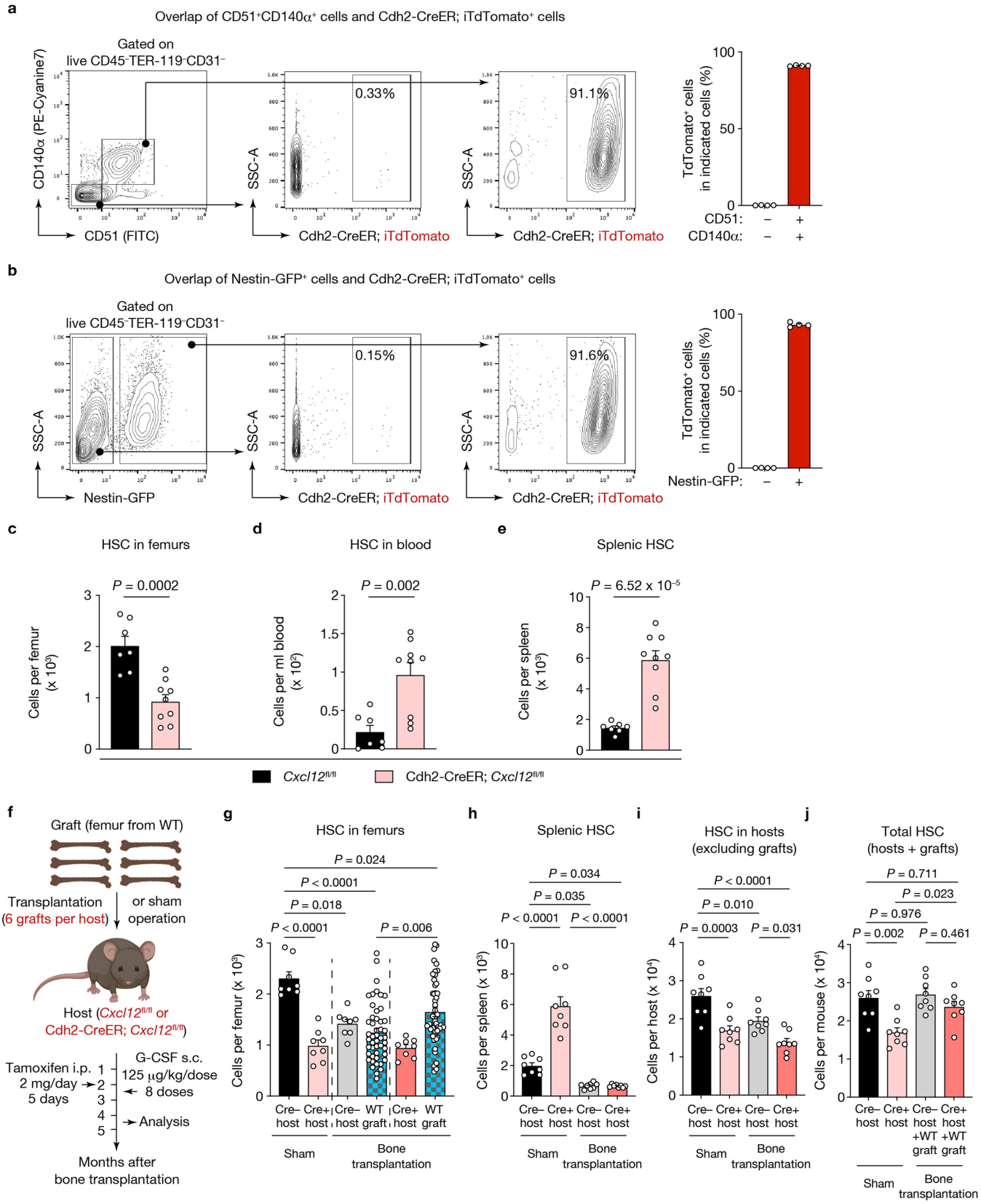

Extended Data Fig. 8 | See next page for caption.

Extended Data Fig. 8 | Total HSC numbers in the body remain unchanged when the size of the intact niche is increased, even in mice with impaired HSC retention in endogenous BM niches. a, Left: representative flow cytometry plots of TdTomato$^+$ cells in CD51$^-$CD140α$^-$ cells and CD51$^+$CD140α$^+$ MSCs within CD45$^-$TER-119$^-$CD31$^-$ fraction of Cdh2-CreER; iTdTomato mice. Right: quantification of overlap of CD51$^-$CD140α$^-$, CD51$^+$CD140α$^+$ and TdTomato$^+$ cells in the CD45$^-$TER-119$^-$CD31$^-$ fraction of Cdh2-CreER; iTdTomato mice. $n = 4$ mice. **b**, Left: representative flow cytometry plots of TdTomato$^+$ cells in Nestin-GFP$^-$ cells and Nestin-GFP$^+$ MSCs within CD45$^-$TER-119$^-$CD31$^-$ fraction of Cdh2-CreER; iTdTomato; Nestin-GFP mice. Right: Quantification of overlap of Nestin-GFP$^-$, Nestin-GFP$^+$ and TdTomato$^+$ cells in the CD45$^-$TER-119$^-$CD31$^-$ fraction of Cdh2-CreER; iTdTomato; Nestin-GFP mice. $n = 4$ mice. **c**-**e**, HSC numbers in the femurs (**c**), blood (**d**) and spleens (**e**) of *Cxcl12*$^{fl/fl}$ and Cdh2-CreER; *Cxcl12*$^{fl/fl}$ mice. $n = 7, 9$ mice, respectively. **f**, Schematic of the transplantation of six WT femurs into Cdh2-CreER; *Cxcl12*$^{fl/fl}$ mice and analyses. The diagram was created using BioRender. Takeishi, S. (2025) https://BioRender.com/9d3nv16. **g**, HSC numbers per host femur and graft of the indicated genotypes. 8 femurs from 8 sham-operated mice, 8 host femurs and 48 grafts from 8 bone transplantation hosts in both *Cxcl12*$^{fl/fl}$ and Cdh2-CreER; *Cxcl12*$^{fl/fl}$ groups. **h**-**j**, HSC numbers in the spleens (**h**), in the entire body of hosts (excluding grafts) (**i**) and the sum of HSCs in the hosts and the grafts (**j**) of the indicated genotypes. $n = 8$ mice per group. Data are mean ± s.e.m. Significance was assessed using a two-tailed unpaired Student's *t*-test (**c**-**e**) or one-way ANOVA (**g**-**j**).

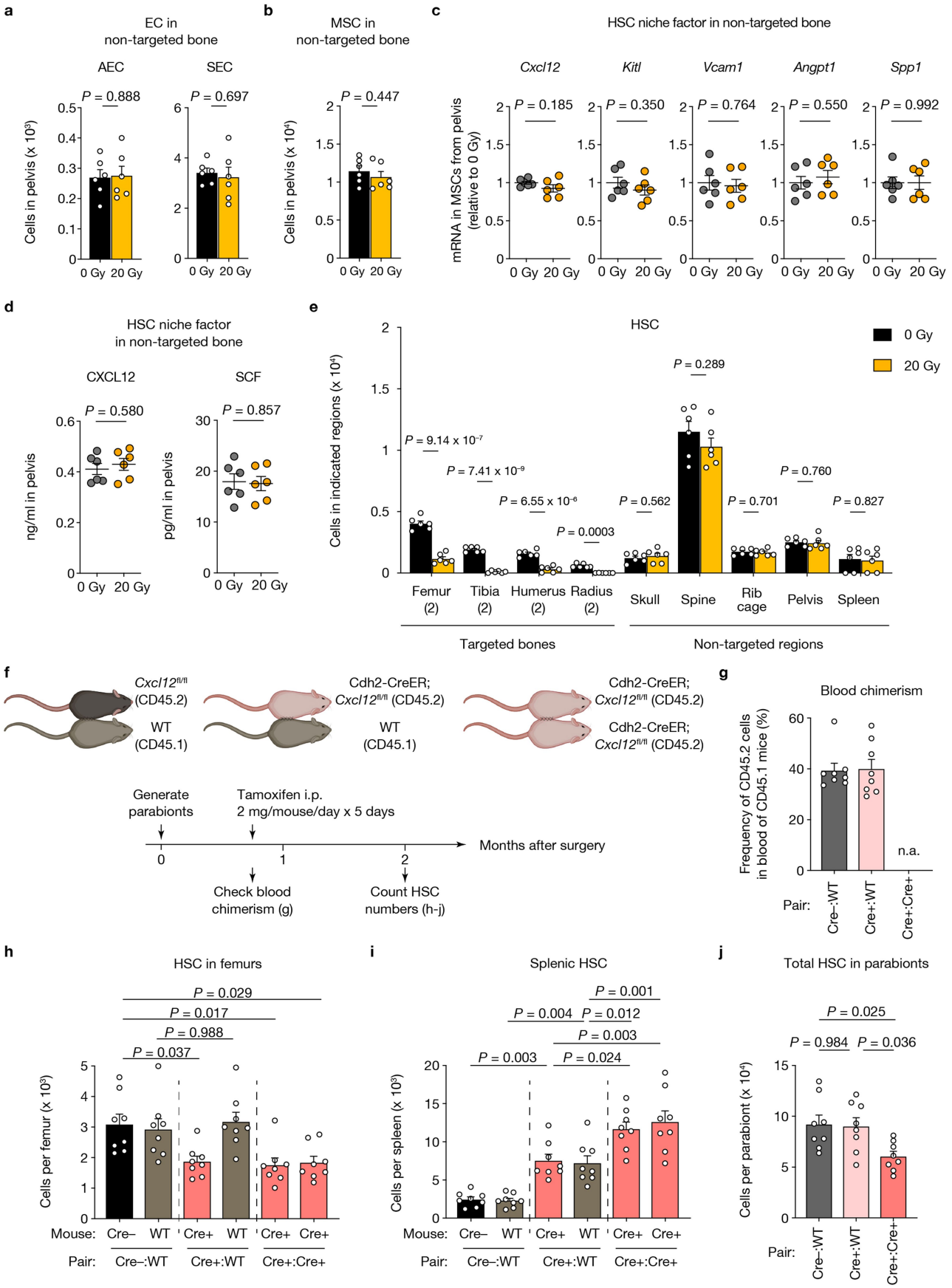

Extended Data Fig. 9 | See next page for caption.

Extended Data Fig. 9 | HSC numbers are restricted at both systemic and local levels. a, **b**, The number of ECs (**a**) and MSCs (**b**) in the non-targeted bone (pelvis) after localized irradiation in the experiment shown in Fig. 3a. *n* = 6 mice per group. **c**, Quantification of mRNA levels of the indicated HSC niche factors in MSCs from the non-targeted bone (pelvis) after localized irradiation. *n* = 6 mice per group. **d**, CXCL12 and SCF levels in BMEF of the non-targeted bone (pelvis) measured by ELISA after localized irradiation. *n* = 6 mice per group. **e**, HSC numbers in the indicated bones and the spleens after localized irradiation. The number in parentheses indicates the number of bones examined per mouse. *n* = 6 mice per group. **f**, Schematic of parabiosis experimental design. The diagram was created using BioRender. Takeishi, S. (2025) https://BioRender.com/9d3nv16. **g**, Percent partner-chimerism in parabionts. n.a.: not available due to expression of the same CD45 isoform. *n* = 8 mice per group. **h**, **i**, HSC numbers per femur (**h**) and spleen (**i**) from mice of the indicated genotypes. 8 mice and 8 partners from 8 parabionts per group. **j**, HSC numbers in the entire bodies per parabiont of the indicated genotypes. *n* = 8 parabionts per group. Data are mean ± s.e.m. Significance was assessed using a two-tailed unpaired Student's t-test (**a**-**e**) or one-way ANOVA (**h**-**j**).

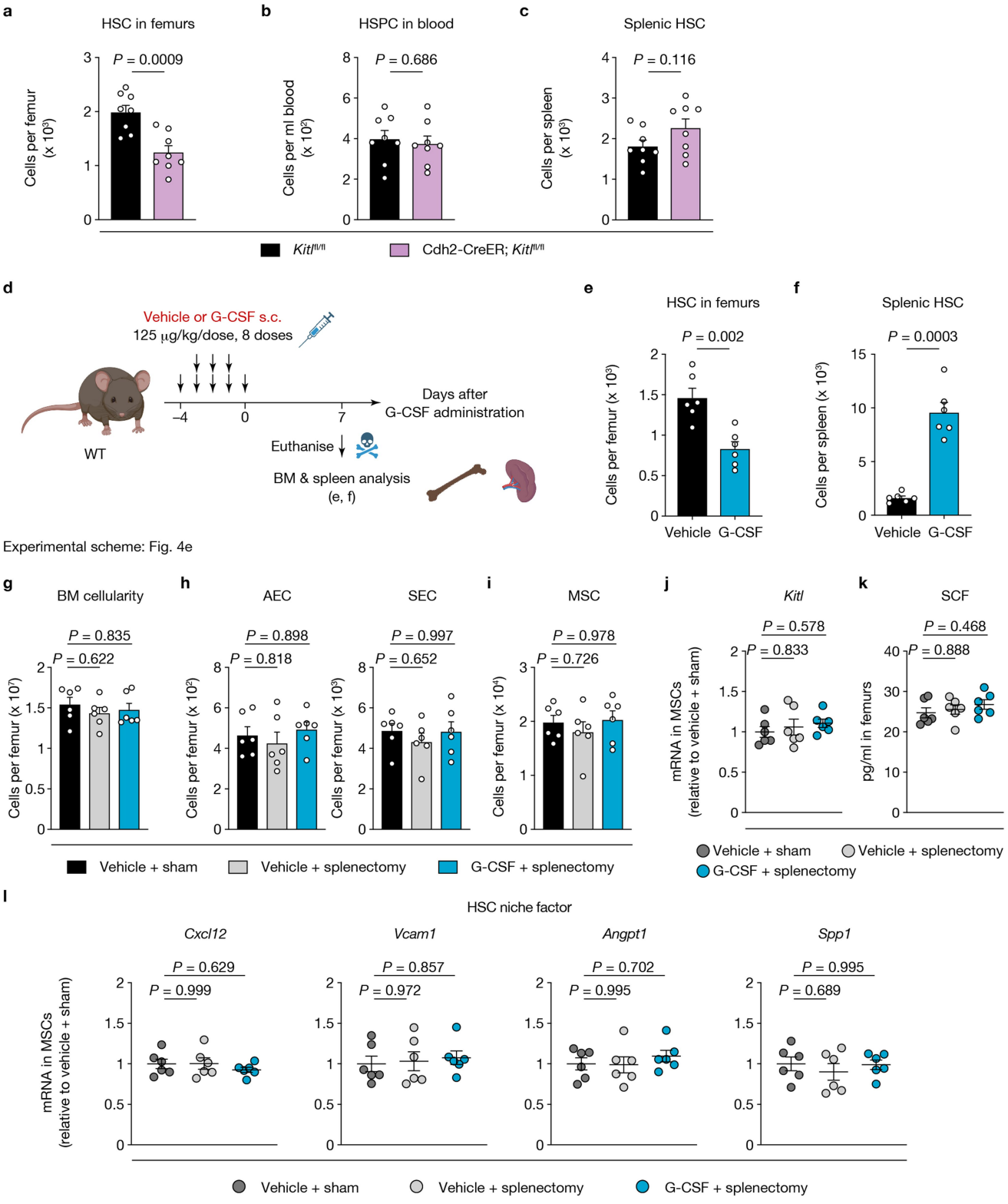

Extended Data Fig. 10 | HSC numbers are not upregulated when they are reduced in specific settings. a, HSC numbers per femur of *Kitl*$^{fl/fl}$ and Cdh2-CreER; *Kitl*$^{fl/fl}$ mice. $n = 8$ mice per group. **b**, HSPC numbers in the blood of *Kitl*$^{fl/fl}$ and Cdh2-CreER; *Kitl*$^{fl/fl}$ mice. $n = 8$ mice per group. **c**, HSC numbers in the spleens of *Kitl*$^{fl/fl}$ and Cdh2-CreER; *Kitl*$^{fl/fl}$ mice. $n = 8$ mice per group. **d**, Experimental strategy to determine HSC numbers in the femurs and the spleens shortly after G-CSF administration. The diagram was created using BioRender. Takeishi, S. (2025) https://BioRender.com/9d3nv16. **e**, **f**, HSC numbers per femur (**e**) and spleen (**f**) at 7 days after vehicle or G-CSF administration in the experiment shown in **d**. $n = 6$ mice per group. **g**-**i**, The number of BM cells (**g**), ECs (**h**) and MSCs (**i**) per femur of the indicated cohorts at 2 months after vehicle or G-CSF administration in the experiment shown in Fig. 4e. $n = 6$ mice per group. **j**, Quantification of *Kitl* mRNA levels in MSCs from the indicated cohorts at 2 months after vehicle or G-CSF administration. $n = 6$ mice per group. **k**, SCF levels in BMEF of the femurs from the indicated cohorts measured by ELISA at 2 months after vehicle or G-CSF administration. $n = 6$ mice per group. **l**, Quantification of mRNA levels of niche factors in MSCs from the indicated cohorts at 2 months after vehicle or G-CSF administration. $n = 6$ mice per group. Data are mean ± s.e.m. Significance was assessed using a two-tailed unpaired Student's *t*-test (**a**-**c**, **e**, **f**) or one-way ANOVA (**g**-**l**).

nature portfolio

Corresponding author(s): Shoichiro Takeishi
Ulrich Steidl

Last updated by author(s): Jun 17, 2025

Reporting Summary

Nature Portfolio wishes to improve the reproducibility of the work that we publish. This form provides structure for consistency and transparency in reporting. For further information on Nature Portfolio policies, see our Editorial Policies and the Editorial Policy Checklist.

Statistics

For all statistical analyses, confirm that the following items are present in the figure legend, table legend, main text, or Methods section.

n/a	Confirmed	
☐	☒	The exact sample size (*n*) for each experimental group/condition, given as a discrete number and unit of measurement
☐	☒	A statement on whether measurements were taken from distinct samples or whether the same sample was measured repeatedly
☐	☒	The statistical test(s) used AND whether they are one- or two-sided *Only common tests should be described solely by name; describe more complex techniques in the Methods section.*
☐	☒	A description of all covariates tested
☐	☒	A description of any assumptions or corrections, such as tests of normality and adjustment for multiple comparisons
☐	☒	A full description of the statistical parameters including central tendency (e.g. means) or other basic estimates (e.g. regression coefficient) AND variation (e.g. standard deviation) or associated estimates of uncertainty (e.g. confidence intervals)
☐	☒	For null hypothesis testing, the test statistic (e.g. *F*, *t*, *r*) with confidence intervals, effect sizes, degrees of freedom and *P* value noted *Give P values as exact values whenever suitable.*
☒	☐	For Bayesian analysis, information on the choice of priors and Markov chain Monte Carlo settings
☒	☐	For hierarchical and complex designs, identification of the appropriate level for tests and full reporting of outcomes
☐	☒	Estimates of effect sizes (e.g. Cohen's *d*, Pearson's *r*), indicating how they were calculated

Our web collection on statistics for biologists contains articles on many of the points above.

Software and code

Policy information about availability of computer code

Data collection	Data collection was performed using SlideBook 6 (Intelligent Imaging Innovations) for confocal microscopy imaging, FACS Diva 6.1 (BD Biosciences) for flow cytometry, and QuantStudio 6 Flex Real-Time PCR System v1.7.2 (Applied Biosystem) for quantitative real-time PCR.
Data analysis	Data analysis was performed using Prism 10 (GraphPad), Excel 16 (Microsoft), SlideBook 6 (Intelligent Imaging Innovations), Fiji build of ImageJ 2 (NIH), FACS Diva 6.1 (BD Biosciences), FlowJo 10 (LLC) and QuantStudio 6 Flex Real-Time PCR System v1.7.2 (Applied Biosystems).

For manuscripts utilizing custom algorithms or software that are central to the research but not yet described in published literature, software must be made available to editors and reviewers. We strongly encourage code deposition in a community repository (e.g. GitHub). See the Nature Portfolio guidelines for submitting code & software for further information.

Data

Policy information about availability of data

All manuscripts must include a data availability statement. This statement should provide the following information, where applicable:

- Accession codes, unique identifiers, or web links for publicly available datasets
- A description of any restrictions on data availability
- For clinical datasets or third party data, please ensure that the statement adheres to our policy

Source data are provided with the paper.

Human research participants

Policy information about studies involving human research participants and Sex and Gender in Research.

Reporting on sex and gender	n/a
Population characteristics	n/a
Recruitment	n/a
Ethics oversight	n/a

Note that full information on the approval of the study protocol must also be provided in the manuscript.

Field-specific reporting

Please select the one below that is the best fit for your research. If you are not sure, read the appropriate sections before making your selection.

☒ Life sciences ☐ Behavioural & social sciences ☐ Ecological, evolutionary & environmental sciences

For a reference copy of the document with all sections, see nature.com/documents/nr-reporting-summary-flat.pdf

Life sciences study design

All studies must disclose on these points even when the disclosure is negative.

Sample size	No statistical method was used to predetermine sample size. Sample size was chosen based on previous studies performed in our laboratory (see references 13, 14, 16, 19, 20, 47).
Data exclusions	No data was excluded from the analysis.
Replication	Experimental replication was attempted at least three times for all datasets/figures shown, and experimental findings were reliably reproduced.
Randomization	Mice were randomly assigned to experimental groups including male and female mice.
Blinding	Investigators were not blinded to mouse genotypes during experiments. Data reported for mouse experiments are not subjective but rather based on quantitative flow cytometry. Data blinding was not possible for some experiments due to obvious difference in expansion or reduction of haematopoietic stem cells.

Reporting for specific materials, systems and methods

We require information from authors about some types of materials, experimental systems and methods used in many studies. Here, indicate whether each material, system or method listed is relevant to your study. If you are not sure if a list item applies to your research, read the appropriate section before selecting a response.

Materials & experimental systems

n/a	Involved in the study
☐	☒ Antibodies
☒	☐ Eukaryotic cell lines
☒	☐ Palaeontology and archaeology
☐	☒ Animals and other organisms
☒	☐ Clinical data
☒	☐ Dual use research of concern

Methods

n/a	Involved in the study
☒	☐ ChIP-seq
☐	☒ Flow cytometry
☒	☐ MRI-based neuroimaging

Antibodies

Antibodies used	The following antibodies were used for immunofluorescence imaging: anti-CD31 Alexa Fluor 647 (MEC13.3; 102516; BioLegend; 5 µg antibody/mouse for injection), anti-CD144 (VE-cadherin) Alexa Fluor 647 (BV13; 138006; BioLegend; 5 µg antibody/mouse for injection).

	Antibodies used for flow cytometry: anti-CD45 APC-eFluor 780 (30-F11; 47-0451-82), anti-TER-119 APC-eFluor 780 (TER-119; 45-5921-82), anti-CD31 PE-Cyanine7 (390; 25-0311-82), anti-CD51 biotin (RMV-7; 13-0512-85), anti-CD140a (PDGFRA) PE (APA5; 12-1401-81), anti-CD140a PE-Cyanine7 (APA5; 25-1401-81), anti-Ly6A/E (SCA-1) FITC (D7; 11-5981-82), anti-Ly-6G/Ly-6C (GR-1) FITC (RB6-8C5; 11-5931-85), anti-Ly-6G/Ly-6C APC-eFluor 780 (RB6-8C5; 47-5931-82), anti-CD11b PE (M1/70; 12-0112-83), anti-CD11b PE-Cyanine7 (M1/70; 25-0112-82), anti-CD11b APC-eFluor 780 (M1/70; 47-0112-82), anti-B220 APC-eFluor 780 (RA3-6B2; 47-0452-82), anti-CD3e APC-eFluor 780 (145-2C11; 47-0031-82), anti-CD48 PerCP-eFluor 710 (HM48-1; 46-0481-85), anti-CD48 PE-Cyanine7 (HM48-1; 25-0481-80), anti-CD41 PerCP-eFluor 710 (MWReg30; 46-0411-82), anti-CD34 eFluor 660 (RAM34; 50-0341-82; 1:50 dilution), anti-CD135 (FLT3) PerCP-eFluor 710 (A2F10; 46-1351-82), anti-CD115 APC (AFS98; 17-1152-82) and anti-CD45.1 PE-Cyanine7 (A20; 25-0453-82) from eBioscience, anti-CD62E PE (10E9.6; 553751) from BD Biosciences, anti-CD117 (cKIT) PE-Cyanine7 (2B8; 105814), anti-CD117 Brilliant Violet 421 (2B8; 105828), anti-CD150 PE (TC15-12F12.2; 115904), F4/80 PE (BM8; 123110) and anti-CD45.2 APC (104; 109814) from BioLegend, and anti-CD3e PerCP-Cyanine5.5 (145-2C11; 65-0031-U100) from Tonbo Biosciences. Streptavidin FITC (11-4317-87) and Streptavidin PerCP-eFluor 710 (46-4317-82) were purchased from eBioscience. Unless otherwise specified, all antibodies, Streptavidin FITC and Streptavidin PerCP-eFluor 710 were used at a 1:100 dilution.
Validation	Antibodies were validated in previous studies performed in our laboratory (see references 13, 14, 16, 19, 20, 47).

Animals and other research organisms

Policy information about studies involving animals; ARRIVE guidelines recommended for reporting animal research, and Sex and Gender in Research

Laboratory animals	B6.Cg-Gt(ROSA)26Sortm14(CAG-tdTomato)/Hze/J (iTdTomato) (#007914), C57BL/6J (CD45.2) (#000664) and B6.SJL-Ptprca Pepcb/BoyJ (CD45.1) (#002014) mice were purchased from The Jackson Laboratory. Nestin-GFP mice were bred in our facility. Cdh5-CreER, Cdh2-CreER, Cxcl12fl/fl, Kitlfl/fl, Tpo–/– and Tg(Alb-Tpo) mice were kindly provided by R. H. Adams (Max Planck Institute for Molecular Biomedicine, Germany), L. Li (Stowers Institute for Medical Research, USA), T. Nagasawa (Osaka University, Japan), S. J. Morrison (University of Texas Southwestern Medical Center, USA), F.J. de Sauvage (Genentech, USA) and W. S. Alexander (The University of Melbourne, Australia), respectively. Unless indicated otherwise, 8–10-week-old mice were used for experiments. All these mice were backcrossed with C57BL/6J mice for more than 10 generations and maintained in pathogen-free conditions under a 12 h/12 h light/dark cycle, at a temperature of 21 ± 1ºC and humidity of 40–70%, and were fed with autoclaved food and water.
Wild animals	No wild animals were used.
Reporting on sex	Both genders were used for experiments.
Field-collected samples	No field-collected samples were used.
Ethics oversight	This study complied with all ethical regulations involving experiments with mice, and all experimental procedures performed on mice were approved by the Animal Care and Use Committee of Albert Einstein College of Medicine.

Note that full information on the approval of the study protocol must also be provided in the manuscript.

Flow Cytometry

Plots

Confirm that:

☒ The axis labels state the marker and fluorochrome used (e.g. CD4-FITC).

☒ The axis scales are clearly visible. Include numbers along axes only for bottom left plot of group (a 'group' is an analysis of identical markers).

☒ All plots are contour plots with outliers or pseudocolor plots.

☒ A numerical value for number of cells or percentage (with statistics) is provided.

Methodology

Sample preparation	Peripheral blood was harvested by retro-orbital bleeding of mice anesthetized with isoflurane and collected in polypropylene tubes containing EDTA. Blood parameters were determined with the Advia120 Hematology System (Siemens). Bone marrow cells were obtained by flushing and dissociating using a 1-mL syringe with phosphate-buffered saline (PBS, Corning) via a 21-gauge needle. For analysis of stromal and endothelial cell populations, intact flushed BM plugs were digested at 37°C for 30 min in 1 mg/mL collagenase type IV (Gibco), 2 mg/mL Dispase (Gibco) and 500 µg/mL DNase I (Sigma-Aldrich) in Hank's balanced salt solution (HBSS, Gibco). These single-cell suspensions were then subjected to red blood cell lysis with ammonium chloride and washed in ice-cold PEB (PBS containing 0.5% BSA and 2 mM EDTA).
Instrument	BD LSRII Special Order System (BD Bioscience) was used for all data acquisition (H55100027). BD FACSAria (BD Biosciences) was used for sorting experiments.
Software	Data was collected using BD FACSDiva 6.1 (BD Biosciences) software. Data was analyzed with FACS Diva 6.1 (BD Biosciences) and FlowJo 10 (LLC) software.
Cell population abundance	Purity of cells sorted or analysed was determined by their appropriate frequency and absolute numbers determined for control wild-type mice according to previous studies. It was described in the literature that haematopoietic stem cells comprise ~0.01% of total bone marrow. We have previously shown that mesenchymal stem cells are ~0.05% of total bone

marrow. In every experiment, we included a control group. Because the sorted populations are very rare, we did not routinely carry out post-sort analysis.

Gating strategy

For all flow cytometric analysis and sorting, dead cells and debris were excluded by forward scatter, side scatter and DAPI (4', 6-diamino-2-phenylindole) staining proflies, following which specific populations were gated according to prior experience with doing similar experiments in our laboratory.

Haematopoietic stem cells were identified as previously described in the literature: negative for lineage (GR-1, CD11b, TER-119, B220, CD3e), negative for CD34 and CD48 and positive for Ly6A/E (SCA-1), CD117 (cKIT) and CD150 (SLAM markers), as depicted in Supplementary Fig. 1b.

All other flow cytometric analyses, donor-derived CD45.2+ cells in transplantation setting, myeloid cells (CD11b+), B cells (B220+) and T cells (CD3e+) have all been described previously (see manuscript for citations describing similar studies done in our laboratory).

☒ Tick this box to confirm that a figure exemplifying the gating strategy is provided in the Supplementary Information.